X-671-65-252

NASA TMX-55236

SOME ASPECTS OF THE FLIGHT DYNAMICS OF THE AEROBEE 350 IN THE REGION OF PITCH-ROLL COUPLING

BY
J. T. LAWRENCE

JUNE 1965

GODDARD SPACE FLIGHT CENTER
GREENBELT, MARYLAND

SOME ASPECTS OF THE FLIGHT DYNAMICS OF THE AEROBEE 350 IN THE REGION OF PITCH-ROLL COUPLING

By

J. T. Lawrence

June 1965

ABSTRACT

The motion in the region of pitch-roll coupling is examined for an Aerobee 350 having a 2^{o} thrust misalignment located in a plane 20^{o} from the reference fin. Nine computer runs are used to illustrate the effects of changing various vehicle characteristics and a discussion is given of the theory involved.

National Aeronautics and Space Administration
Goddard Space Flight Center
Greenbelt, Maryland

TABLE OF CONTENTS

LIST OF ILLUSTRATIONS

LIST OF ILLUSTRATIONS (Continued)

is very nearly equal to the actual roll rate obtained from the equations of motion on the computer. Equation (3) is obtained by setting equation (2) equal to zero, since $\dot{p}$ will be zero when steady-state is reached, and solving for the roll rate (p) which is now the steady-state roll rate. Looking again at equation (2) and equation (1), it can be seen that since the sum $L(\delta) + L(p) = I_x\dot{p} > 0$ is so small, only a small negative value of the induced roll moment is necessary in order to cause $\dot{p}$ to go to zero or become negative. The pitch rate is decreasing in the vicinity of resonance ($\dot{\omega} < 0$) and, in order for the vehicle to lock-in ($p = \omega$), it is necessary that $\dot{p} = \dot{\omega} < 0$. Under such conditions, equation (1) becomes

$$L(\delta) + L(p) + L(\text{induced}) = I_x\dot{p} = I_x\dot{\omega} < 0 \qquad (4)$$

In order for the vehicle to see an induced roll moment it is necessary for the total angle of attack to be greater than zero. A misalignment or asymmetry in the vehicle will give it a non-rolling trim angle. When the vehicle is rolling this non-rolling trim angle will be magnified by a factor as shown in Figure (7). This magnification factor is the ratio of the rolling trim angle to the non-rolling trim angle and is dependent on the frequency ratio and the amount of damping available. Figure (7) shows that the magnification factor is unity when the frequency ratio is zero ($p = 0$). As the frequency ratio starts to increase the magnification factor slowly increases until the frequency ratio nears the resonance region ($p/\omega = 1$). In this region the non-rolling trim angle is magnified in a fashion depending on the available damping in the system. For air vehicles the damping is usually such that large increases in the total angle of attack can occur at resonance. After the passage through resonance the magnification factor quickly decreases to values much less than unity as the frequency ratio increases. The non-rolling trim can come from such factors as thrust misalignment, fin misalignment, mass asymmetry, and vehicle configuration asymmetries. Since one or more of these will invariably be present, it is necessary to learn as much as possible about the magnitudes and directions which may be expected for each one. If the non-rolling trim is sufficiently large the total angle of attack of the vehicle can be magnified to the point where the induced roll moment can have significant effects on the roll behavior of the vehicle.

Another important factor is the phase shift in the aerodynamic roll angle which occurs between launch and resonance. The aerodynamic roll angle is the phase angle from vibrations theory and a representative sketch is shown in Figure (8). It is given by

$$\tan \phi' = \frac{\tan\beta}{\tan\alpha} \qquad (5)$$

INTRODUCTION

This report presents an analysis of nine computer runs selected from the "Aerobee 350 Roll-Yaw Coupling Study", reference (1). This study was performed by Space General Corporation for the Goddard Space Flight Center. The configuration used is shown in Figure (1), and the nominal trajectory parameters are given in Figures (2) through (5). The runs selected for this analysis all had a 2^{o} thrust misalignment oriented in a plane 20^{o} from the reference fin as shown in Figure (6) and, therefore, serve to illustrate the effects of various parameters on the behavior of the vehicle during and after pitch-roll coupling.

The analysis is based on the theory expressed by the author in reference (2), a portion of which is included below for completeness.

THEORY

The roll equation of motion may be written as

$$L(\delta) + L(p) + L(\text{induced}) = I_x \dot{p} \qquad (1)$$

This says that the sum of the roll driving, roll damping, and induced roll moments is equal to the product of the roll moment of inertia times the roll acceleration. Under normal flight conditions the roll driving moment is positive, the roll damping moment is negative, and the sign of the induced roll moment is a function of the aerodynamic roll angle, total angle of attack, and Mach number. For the Aerobee 350 study, theoretical means were used to determine the roll driving and roll damping moments. The methods used did not consider the effects of aerodynamic roll angle and total angle of attack, therefore, in this study the roll driving moment is always positive and the roll damping moment is always negative. This is not a necessarily valid situation, but it is the best available at this time, and is perfectly adequate from the theoretical point of view for studying resonance phenomena. The induced roll moments were obtained in a static wind tunnel test conducted at the Jet Propulsion Laboratory.

Until a vehicle has reached its equilibrium roll rate the absolute value of the roll driving moment will exceed that of the roll damping moment. If the total angle of attack is zero, equation (1) becomes

$$\overset{(+)}{L(\delta)} + \overset{(-)}{L(p)} = I_x \dot{p} > 0 \qquad (2)$$

For the Aerobee 350 studied the fin cant angle was only 0.312^{o}. This small cant angle results in a situation in which the roll driving moment is only slightly larger than the roll damping moment in absolute value. In fact, until some time past resonance when the dynamic pressure is low, a calculation of the steady-state roll rate at any point in the trajectory from

$$p_{ss} = -\frac{C_{l_\delta}\delta}{C_{l_p}\frac{d}{2V}} = -\frac{L_\delta \delta}{L_p} \qquad (3)$$

When $p = \omega$, $\emptyset'$ remains constant and the vehicle is "locked-in". The sketch shows that $\emptyset'$ changes very slowly from the initial trim plane until the motion is near resonance. The aerodynamic roll angle then increases its rate of change, passes through resonance at a point 90° away from the original trim plane, and then settles out near 180° from the original trim plane as the frequency ratio continues to increase above resonance. The sketch represents the steady-state case with adequate damping and insignificant transients introduced at resonance. In the case of the Aerobee 350 this is not quite the situation. Due to the dynamics of the flight and the rapidly changing environment, the aerodynamic roll angle shift of 90° as well as the maximum magnification of the total angle of attack occur slightly after resonance. Also, since the damping is low after resonance and the transients can be sizeable, the $\emptyset'$ motion above resonance shows appreciable evidence of the transient roll response superimposed on the steady-state motion. The region below resonance, however, has adequate damping and, after the launch and booster separation transients have been damped, the aerodynamic roll angle history up to resonance is as shown in the sketch.

The importance of this phase shift lies in the fact that the initial trim plane will be determined by the direction of the resultant misalignment causing the non-rolling trim angle. This determines, therefore, the region in which the aerodynamic roll angle will be near resonance when the non-rolling trim angle is receiving large magnification, thereby producing large induced roll moments. Figures (9) and (10) show the induced roll moment coefficient. Depending on where the aerodynamic roll angle is on the vehicle the induced roll moments may be helpful or detrimental. The orientation and size of the resultant misalignment on the vehicle are, therefore, very important factors in determining whether or not lock-in will occur.

In reference (3), Nicolaides discusses the importance of the side moment induced on the vehicle by the same conditions which cause the induced roll moment. He shows that a positive side moment will decrease the damping while a negative side moment will increase the damping. Since a negative induced roll moment is needed for roll lock-in, the sign of the side moment is important in those aerodynamic roll angle regions where the induced roll moment is negative. For the Aerobee 350 the side moment is negative in these regions when the total angle of attack is lower than the crossover point of the induced roll moment as seen in Figure (11).

It will be noted that the nearly constant value of the aerodynamic roll angle up to the resonance region results in the vehicle being in a near lunar motion. This means that the plane of the vehicle which is facing the wind vector is remaining close to the initial trim plane until the vicinity of resonance. This is not the lunar motion at the nutation frequency which gives rise to the possibility of catastrophic yaw as discussed in reference (3), but it is the nearly steady-state motion whose frequency is equal to the roll rate which is the driving frequency. Side moments are practically non-existent in this region since the total angles of attack are small.

ANALYSIS

The computer runs are listed here with their actual case numbers from reference (1). In order to follow the motion description, a sketch of the trend of the induced roll moment as a function of the aerodynamic roll angle is shown in Figure (12).

CASE 20

This case was run using linear rigid body aerodynamics which means that there were no induced roll or side moments to affect the vehicle motion, and lock-in could not occur. It serves, therefore, as a nominal case to which the others may be compared. Figure (13) shows the undisturbed passage of the roll rate through resonance and, due to the use of linear aerodynamics, the linear pitch rate is the actual pitch rate for the flight. Also, it is not until after resonance that the difference between the actual roll rate and the steady-state calculation becomes noticeable. Resonance occurs at about 31.3 seconds.

In Figure (14) the total angle of attack is seen to grow to a maximum of 6.75° at 34 seconds and then drop off sharply as the frequency ratio increases above 1.0 and the magnification factor rapidly decreases. Also shown in this figure is the non-rolling trim angle of attack.

Figure (15) shows the aerodynamic roll angle as a function of time. It shows the aerodynamic roll angle at resonance ($t \approx 31.3$ sec.) to be about 70° which, starting from 20°, is a phase shift of only 50°. A $\emptyset'$ of 110° (90° phase shift) is not reached until about 32.5 seconds. This lag in the phase shift, and a similar lag in the peak magnification of the total angle of attack, is due to the fact that the computer results include the rapidly changing environment, flight parameters, and aerodynamic characteristics of the vehicle, so that these results lag those which would be obtained under constant conditions. This figure also demonstrates the significance of the low damping available after resonance. This is evident in that the roll motion does not settle out at a phase shift of nearly 180°, but continues to show the transient effects superimposed on the steady-state motion.

CASE 12

This case includes the non-linear aerodynamics and elastic body center of pressure. The resulting motions are shown in Figures (16), (17), and (18). At $t = 26.0$ sec. the roll rate is proceeding in the usual manner toward resonance, the non-rolling trim angle is essentially unmagnified, the aerodynamic roll angle has only shifted about 15°, and the roll acceleration is very low.

Now, as the motion gets to about t = 29.0 sec., the non-rolling trim angle is being magnified by a factor of two, and the aerodynamic roll angle is near 55^{o}. At this point the induced roll moment is significant and positive resulting in the increase in $\dot{p}$. At t = 29.8 sec., however, the aerodynamic roll angle passes through 90^{o} and the induced roll moment becomes negative. Also, the total angle of attack has increased to about 4^{o} so that the size of the induced roll moment has also increased. The result is that $\dot{p}$ suddenly becomes negative and, since the roll rate is near resonance with the pitch rate, the vehicle proceeds to lock-in at an aerodynamic roll angle of about 105^{o}. For this particular case the resonant value of the aerodynamic roll angle should be $20^{o} + 90^{o} = 110^{o}$. This represents, however, a portion of the roll curve where the induced roll moment is near neutral stability, whereas 105^{o} is in the stable region. Also, the value of the induced roll moment at 105^{o} is that which is necessary for roll lock-in. As the total angle of attack increases the induced roll moment at first increases on the negative side and then starts to decrease on the negative side as can be seen in Figure (9). As the maximum total angle of attack is reached the induced roll moment is still negative, but the vehicle is able to break-out of the locked-in condition. It can do so because, even though the induced roll moment is negative, it has decreased in magnitude and is no longer able to overcome the sum of the roll driving and roll damping moments. This sum has increased during lock-in because the roll rate is decreasing and the roll damping moment is directly proportional to the roll rate, therefore, it also decreases in magnitude.

Coincident with the break-out, the total angle of attack decreases due to the decreasing magnification factor above resonance. The small oscillations between t = 33.5 seconds and t = 36.0 seconds are due to the fact that the total angle of attack is still large enough to cause significant induced roll moments, but the sign of these moments is changing because the aerodynamic roll angle is undergoing a transient motion due to the large disturbances caused by the resonant situation, and the decreasing damping due to increasing altitude. From this point, the roll rate continues toward sustainer burnout in the usual fashion, and the total angle of attack damps to a small value.

This case is an excellent example of lock-in and break-out and the reasons given for the motions will apply for the rest of the cases to be discussed.

CASE 21

This case illustrates the importance of the side moment in damping the angular motion of the vehicle. This run is the same as case 12 except that the side force and moment are equal to zero. Referring to Figures (19), (20), and (21), the motion until lock-in occurs is the same as case 12. Once lock-in has occurred, however, $\dot{\omega}$ is seen to be more negative than in case 12 thereby causing $\dot{p}$ also to be more negative. This happens because the side moment is not available to help damp the total angle of attack which is able, therefore, to

grow more rapidly than before. This higher total angle of attack time history gives lower absolute values for the pitch frequency. When the vehicle is able to start break-out at about t = 31.5 seconds, the total angle of attack is already up to 10^{o}. The roll rate increases for about 0.3 seconds and then at t = 31.8 seconds it rapidly decreases, passing through zero at about t = 31.9 seconds. At the same time the total angle of attack is seen to grow to the vicinity of 30^{o}, at which point the computer cuts off due to lack of aerodynamic data. The reasons for this behavior can be explained by observing that soon after break-out the aerodynamic roll angle passes through 135^{o} where a sign change occurs in the induced roll moment. At low total angles of attack the sign would now be positive, however, the total angle of attack is now so high that the trend shown in Figure (12) no longer holds, but is in fact reversed. This means that after $\emptyset'$ has passed 135^{o} the induced roll moment has a very large negative value which, in conjunction with the roll damping moment, completely overrides the driving moment and causes the observed roll rate behavior.

The obvious conclusion from comparing this case with case 12 is that the side moment is a very important factor in considering roll lock-in, and that the aerodynamics of the Aerobee 350 are such that the side moment aids the damping of the angular motion under normal conditions (i.e., low total angles of attack).

CASE 66

Due to an oversight the pitch damping coefficients used in the study were only one-half of the values which should have been used. When this was discovered it was decided to run case 12 with the correct pitch damping in order to determine the effects of this error. The results are shown in Figures (22), (23), and (24) which can be compared with Figures (16), (17), and (18) from case 12. Until lock-in occurs the two cases are the same. During lock-in case 66 shows a less negative $\dot{\omega}$ which is due to the higher pitch damping that holds the total angle of attack down and, therefore, results in a higher absolute value of the pitch frequency. The maximum total angle of attack reached is about 13% less than case 12 and break-out starts about one second earlier.

CASE 37

In this case the roll driving coefficient slope (C_{ℓ_δ}) and the roll damping coefficient slope (C_{ℓ_p}) have been taken at one-half of their nominal values. Otherwise the inputs are identical to case 12. As can be seen in Figures (25), (26), and (27) the vehicle total angle of attack builds up to the point where it exceeds the program limit. This is quite different from case 12 where the vehicle remains stable and the total angle of attack damps to a small value following break-out. In order to understand what happened in this case it should be examined in conjunction with case 12.

Since the values of the roll coefficient slopes (C_{l_δ} and C_{l_p}) are only half of their nominal values, the sum $L(\delta)+L(p)$ up until the occurrence of lock-in will only be one-half of that previously encountered. Therefore, at any given total angle of attack and aerodynamic roll angle, the induced roll moment will be twice as effective when it is taken into consideration. Also, only one-half of the usual required value of the induced roll moment is needed in order to establish roll lock-in. This can be seen in Figure (27) which shows the lock-in roll angle to be between 95° and 100° rather than at 105° as in case 12. This roll angle is close to the symmetry point of 90° and the induced roll moment is correspondingly low. For the same reason the vehicle also has a lower side moment at a given total angle of attack which results in a smaller amount of damping, and, consequently, the total angle of attack is able to grow more rapidly. Break-out of the aerodynamic roll angle occurs at about 32 seconds. The roll rate plot shown in Figure (25) shows that the roll rate has already started to increase by this time. This is due to an oscillation of the aerodynamic roll angle just prior to its break-out which approaches 90° where the induced roll moment is nearly zero and the vehicle, therefore, is able to momentarily increase its roll rate. As break-out starts at t = 32.0 seconds, however, the aerodynamic roll angle moves into a region where high induced roll moments exist due to the still large value of the total angle of attack. This causes a decrease in the roll rate until t = 32.4 seconds at which time the roll rate increases up to the vicinity of the nominal roll rate and oscillates about this value. The large amplitude of these oscillations is due to the large induced roll moments which are acting on the vehicle.

Corresponding to the break-out of the roll rate, the total angle of attack starts to decrease as it did in case 12. Initially, this decrease is due to the lower magnification as the frequency ratio increases above resonance, and also to the side moment which is negative in this region of the aerodynamic roll angle ($90^\circ < \phi' < 135^\circ$), thereby helping to damp the motion. At about 32.6 seconds, however, ϕ' passes through 135° and the side moment becomes positive and starts decreasing the damping. At t = 32.9 seconds, the damping can no longer contain the motion and the total angle of attack again increases. At t = 33.2 seconds the aerodynamic roll angle exceeds 180° and the side moment becomes a stabilizing influence again; however, by this time the total angle of attack is up to 9° and the vehicle is passing through the condition of neutral static stability due to the forward shift in center pressure as the total angle of attack increases. As Figure (26) demonstrates, the stabilizing effect of the side moment at this time contributes too little, too late; and the vehicle becomes unstable.

CASE 59

This case is the same as case 12 except that the fin cant angle has been reduced by 10% as has the initial roll rate. The resulting motions are shown in Figures (28), (29), and (30). Due to the lower value of the nominal roll rate at any given flight time, when compared to case 12, resonance occurs at a later time in the flight, t = 30.5 seconds, as shown in Figure (28). The total angle of attack at resonance, Figure (29), is somewhat higher than in case 12 and the resulting lock-in value for the aerodynamic roll angle, Figure (30), is in the vicinity of 100^{o} rather than 105^{o}. This means that at a given total angle of attack during lock-in the side moment in this case will be less than that in case 12. As a result, even though break-out occurs around t = 33.5 seconds, the total angle of attack growth is such that the available damping cannot prevent the vehicle from becoming statically unstable.

CASE 62

This case is identical to case 12 in all respects except that the fin cant angle has been increased by 10% as has the initial roll rate. As shown in Figure (31), resonance occurs earlier than in case 12 due to the higher roll rate. Comparison of Figure (32) with Figure (17) shows that the total angle of attack history about the resonance point is lower for case 62. In addition, Figure (33) shows that the vehicle does not completely lock-in as did case 12. Also, in the resonance region, the aerodynamic roll angle is as large as or greater than that in case 12. This results in a larger stabilizing side moment which retards the total angle of attack growth. When break-out occurs, therefore, the vehicle still has sufficient static stability so that the total angle of attack is damped to a relative low value above resonance.

CASE 30

This run differs from case 12 in that a non-linear rigid body center of pressure was used in place of the non-linear elastic body center of pressure. The results are shown in Figures (34), (35), and (36). Comparison of Figure (34) with Figure (16) shows that both lock-in and break-out occur later in case 30. This is due to the higher pitch rate time history which results in the rigid body situation. This higher pitch rate is caused by the increase in distance of the center of pressure from the center of gravity when the elastic effects are neglected.

Figure (35) shows the lock-in aerodynamic roll angle to be about 105^{o} which is the same as case 12. Figure (36) shows the peak total angle of attack to be about 8.4^{o} at t = 35.1 seconds, whereas in case 12 the maximum was 8.1^{o} at t = 33.9 seconds. This difference is caused by the later occurrence of resonance in case 30 and the resulting lower value of damping available due to the higher altitude.

CASE 64

This case differs from case 12 in that the center of gravity has been moved 0.5 calibers aft, thus decreasing the static margin by this constant value over the entire flight. This decrease in static margin compared to case 12 results in a lower pitch rate time history, thereby causing resonance to occur earlier, Figure (37). In Figure (39) the aerodynamic roll angle is seen to behave very similar to case 62 in that complete lock-in does not occur. Even so, the reduced static margin causes static instability to occur at about 31.6 seconds and the total angle of attack, Figure (38), continues to build up to the machine cut-off value of 30^{o}.

SUMMARY

This analysis has demonstrated the importance of looking at all of the factors which can contribute to the motions of a vehicle in the region of pitch-roll coupling. These nine (9) computer runs give a good insight into the effects of both large and small changes in various vehicle parameters. Application of the physical picture presented herein should be a valuable tool in analyzing the motion of any vehicle affected by pitch-roll coupling.

REFERENCES

(1) Sollow, P. A., "Aerobee 350 Roll-Yaw Coupling Study", Final Report 379RC-2 (3 volumes), Space General Corporation, December 1964. (Contract No. NAS 5-3313 for NASA/Goddard Space Flight Center.)

(2) Lawrence, J. T., "Flight Dynamics of Sounding Rockets in the Region of Pitch Roll Coupling", X-671-65-183, NASA/Goddard Space Flight Center. March 1965.

(3) Nicolaides, J. D., "Missile Flight and Astrodynamics", Technical Note 100A, Bureau of Naval Weapons, 1961.

NOMENCLATURE

C_{l_p}	Roll damping coefficient slope $dC_l/d(\frac{pd}{2V})$
C_{l_δ}	Roll driving coefficient slope $dC_l/d\delta$
d	Body diameter
I	Pitch and yaw moment of inertia
I_x	Roll moment of inertia
L(induced)	Induced roll moment
L(p)	Roll damping moment
$L(\delta)$	Roll driving moment
M	Mach number
$M(\eta)$	Pitching moment ($= M_\eta \eta$)
p	Roll rate
$\dot{p}$	Roll acceleration
p_{ss}	Steady-state roll rate
t	Time
V	Velocity
α	Angle of attack (body axes)
β	Angle of sideship (body axes)
δ	Fin cant angle
η	Total angle of attack ($=\sqrt{\alpha^2+\beta^2}$)
ϕ'	Aerodynamic roll angle ($= \tan^{-1}\frac{\tan}{\tan}$)
ω	Pitch rate ($= \sqrt{\frac{M(\eta)}{\eta I}}$)

AEROBEE 350 CONFIGURATION STUDIED
BY SPACE GENERAL CORP. FOR
NASA/GODDARD SPACE FLIGHT CENTER

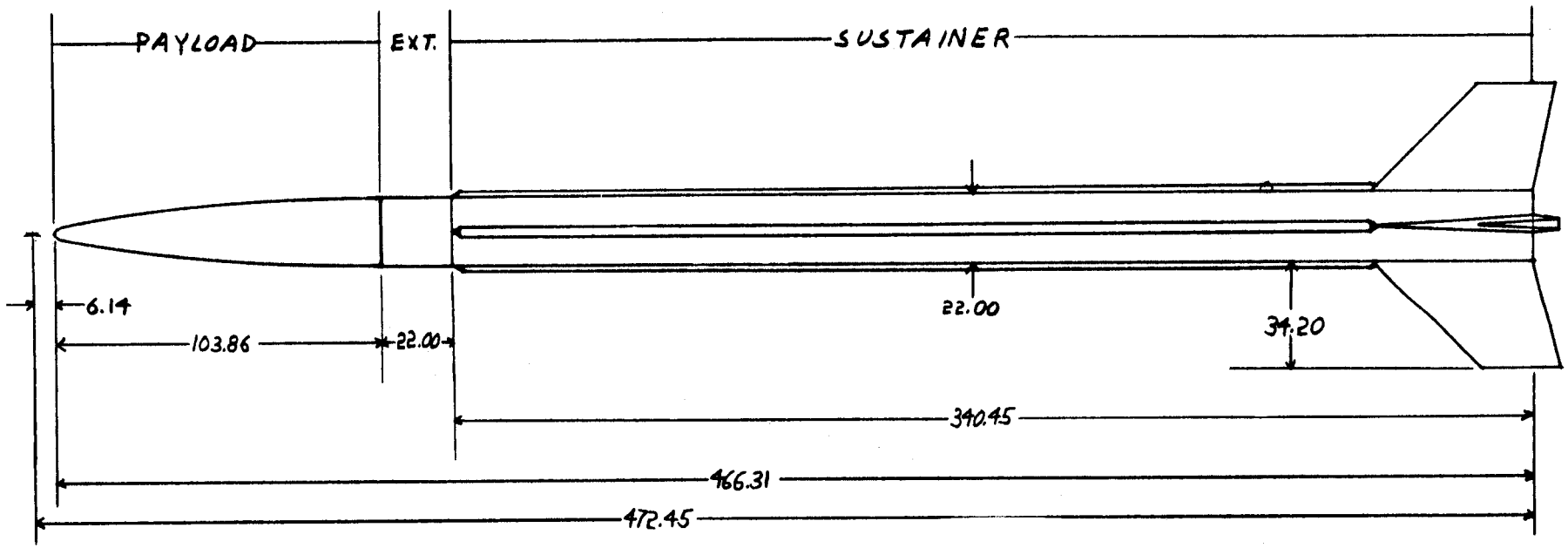

ALL DIMENSIONS ARE INCHES

FIGURE 1.

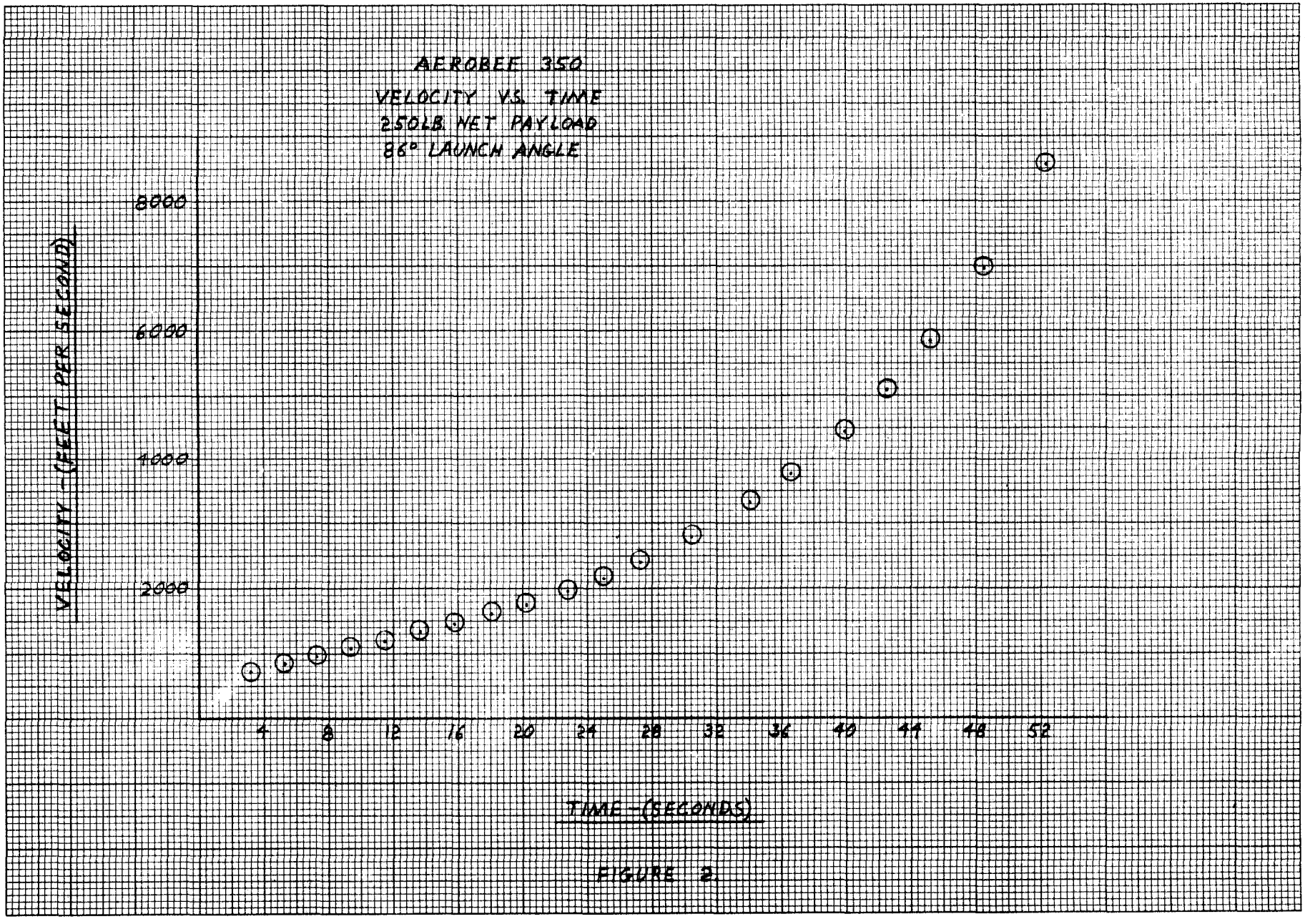
AEROBEE 350
VELOCITY V.S. TIME
250LB. NET PAYLOAD
86° LAUNCH ANGLE
VELOCITY - (FEET PER SECOND)
8000
6000
4000
2000
4
8
12
16
20
24
28
32
36
40
44
48
52
TIME - (SECONDS)

FIGURE 2.

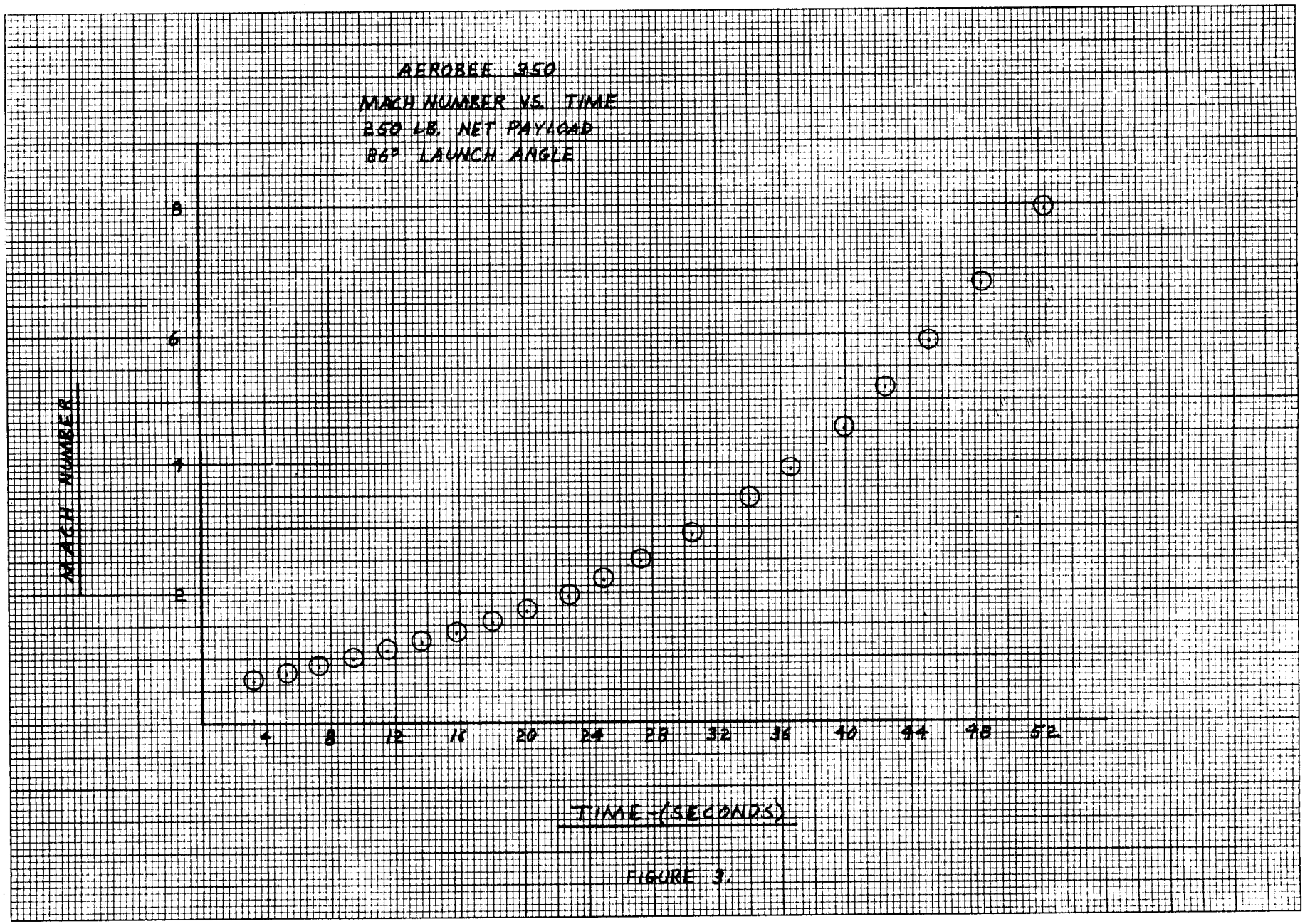
AEROBEE 350
MACH NUMBER VS. TIME
250 LB. NET PAYLOAD
86° LAUNCH ANGLE
MACH NUMBER
8
6
4
2
4
8
12
16
20
24
28
32
36
40
44
48
52
TIME - (SECONDS)

FIGURE 3.

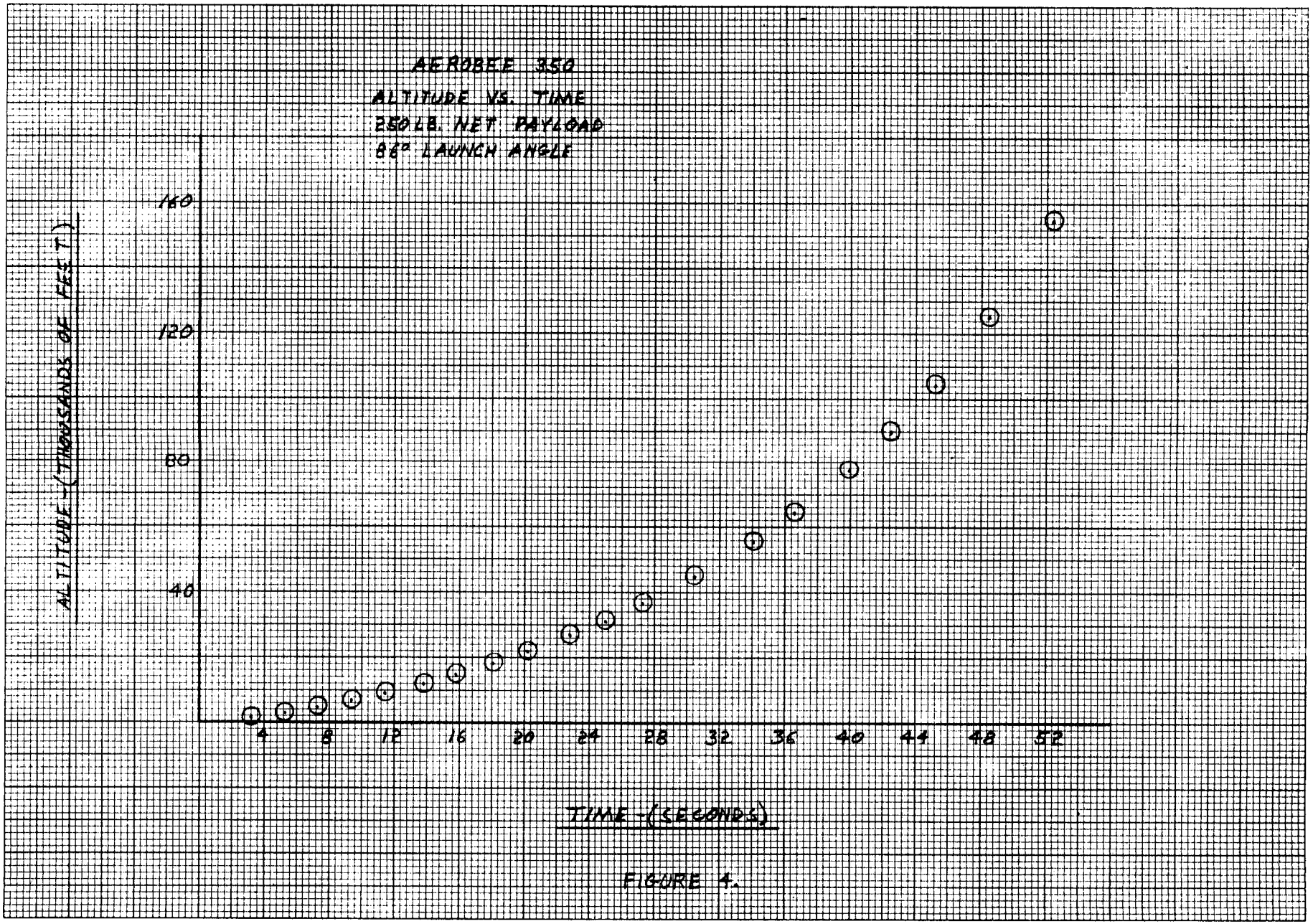
AEROBEE 350
ALTITUDE VS. TIME
250 LB. NET PAYLOAD
86° LAUNCH ANGLE
ALTITUDE - (THOUSANDS OF FEET)
160
120
80
40
4
8
12
16
20
24
28
32
36
40
44
48
52
TIME - (SECONDS)

FIGURE 4.

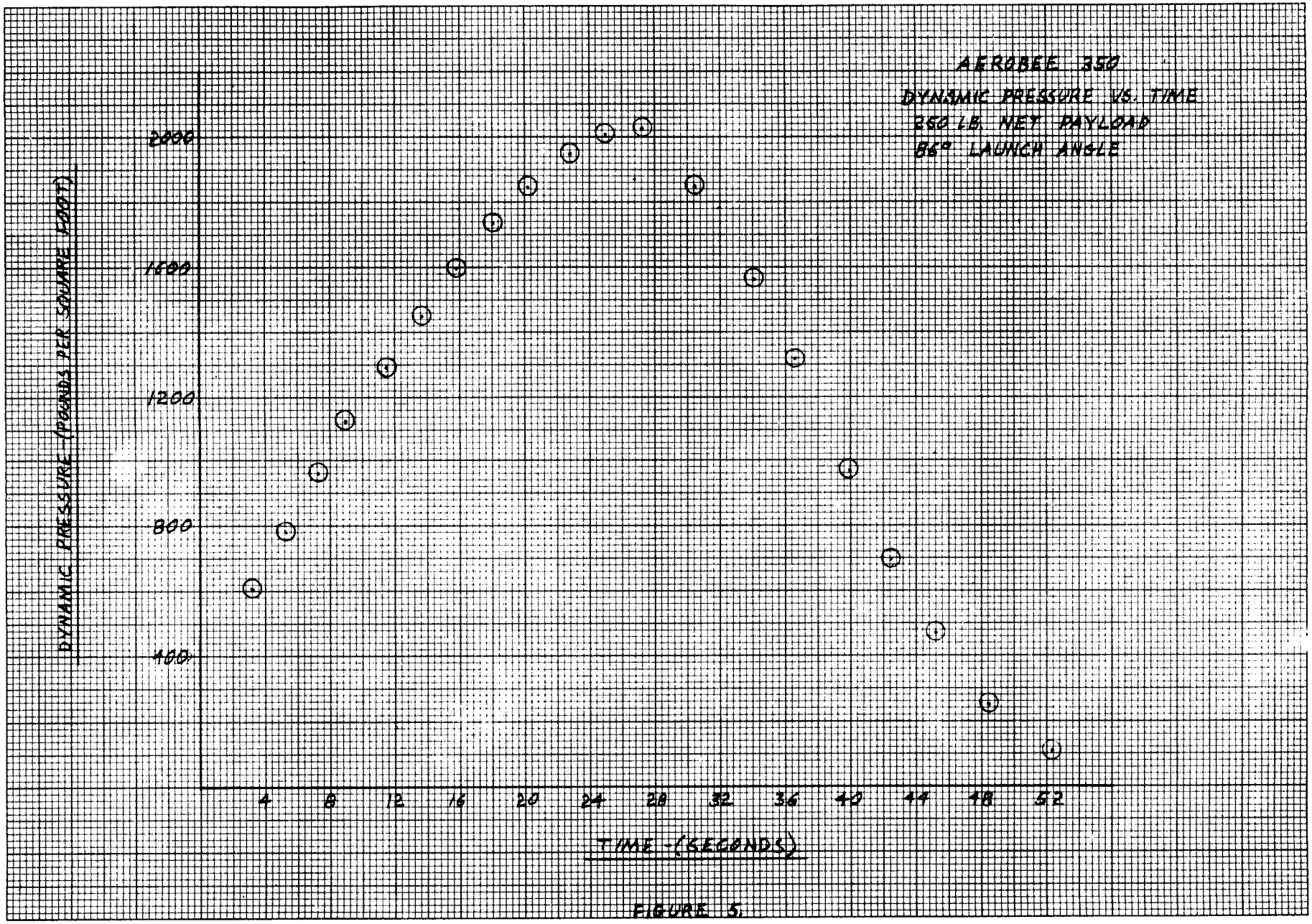
AEROBEE 350
DYNAMIC PRESSURE VS. TIME
250 LB. NET PAYLOAD
86° LAUNCH ANGLE
DYNAMIC PRESSURE - (POUNDS PER SQUARE FOOT)
2000
1600
1200
800
400
4
8
12
16
20
24
28
32
36
40
44
48
52
TIME - (SECONDS)

FIGURE 5.

AEROBEE 350 WITH THRUST MISALIGNMENT IN A PLANE 20° FROM THE REFERENCE FIN SO AS TO GIVE A NOSE-UP MOMENT IN THE NON-ROLLING CONDITION

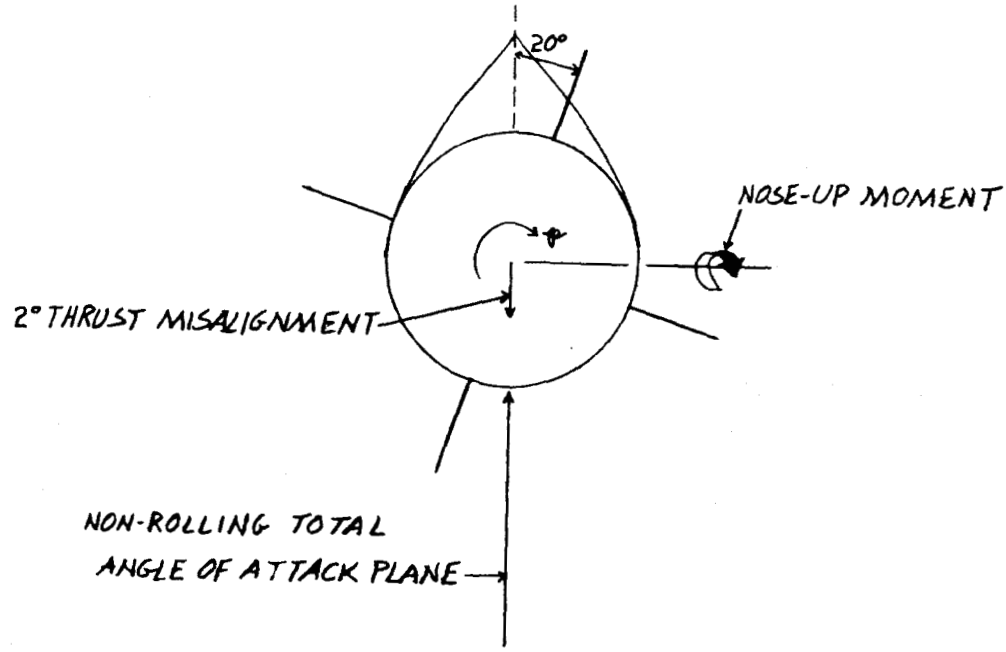

FIGURE 6.

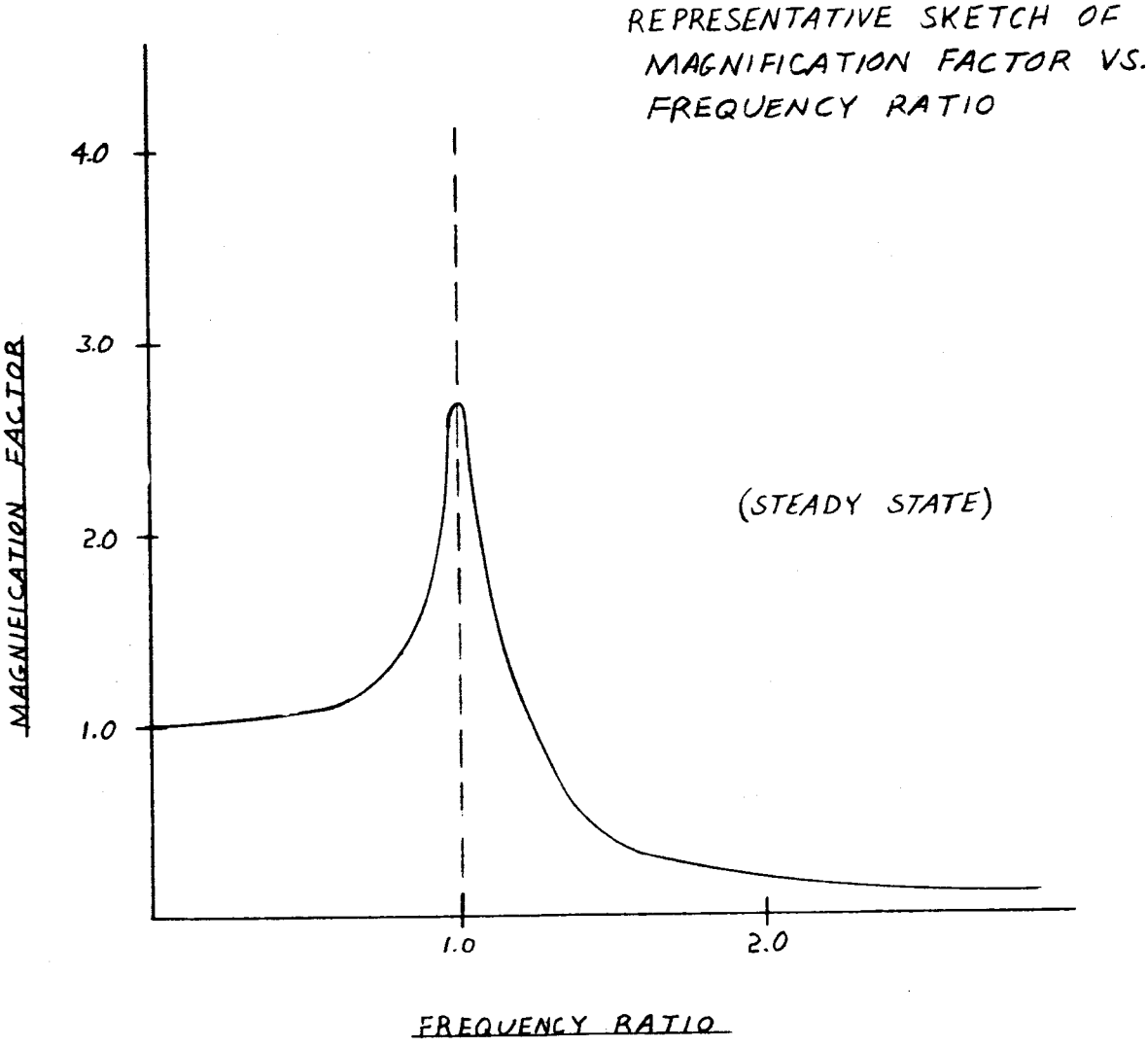
REPRESENTATIVE SKETCH OF
MAGNIFICATION FACTOR VS.
FREQUENCY RATIO
(STEADY STATE)
MAGNIFICATION FACTOR
4.0
3.0
2.0
1.0
1.0
2.0
FREQUENCY RATIO

FIGURE 7.

REPRENTATIVE SKETCH OF
PHASE ANGLE VS FREQUENCY RATIO

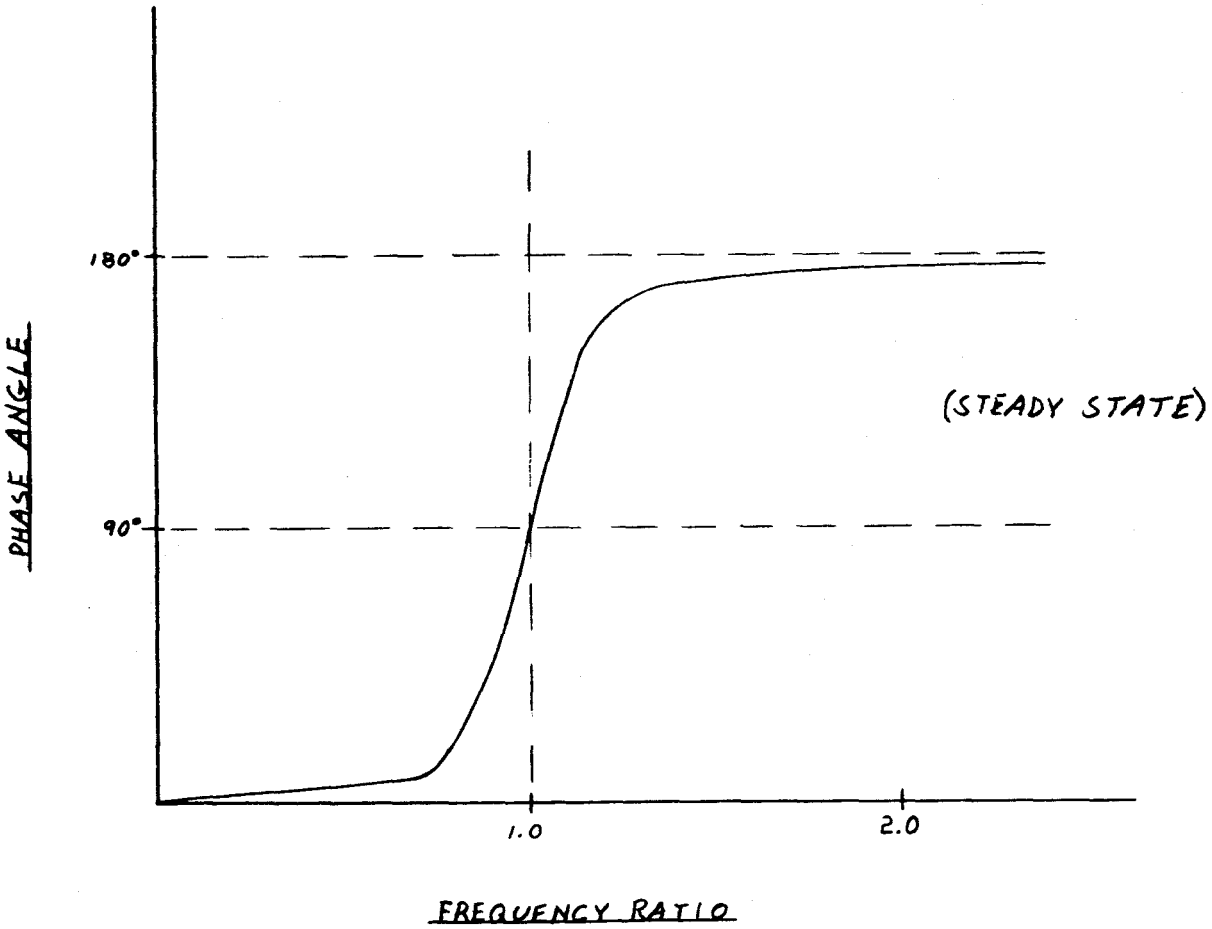

FIGURE 8.

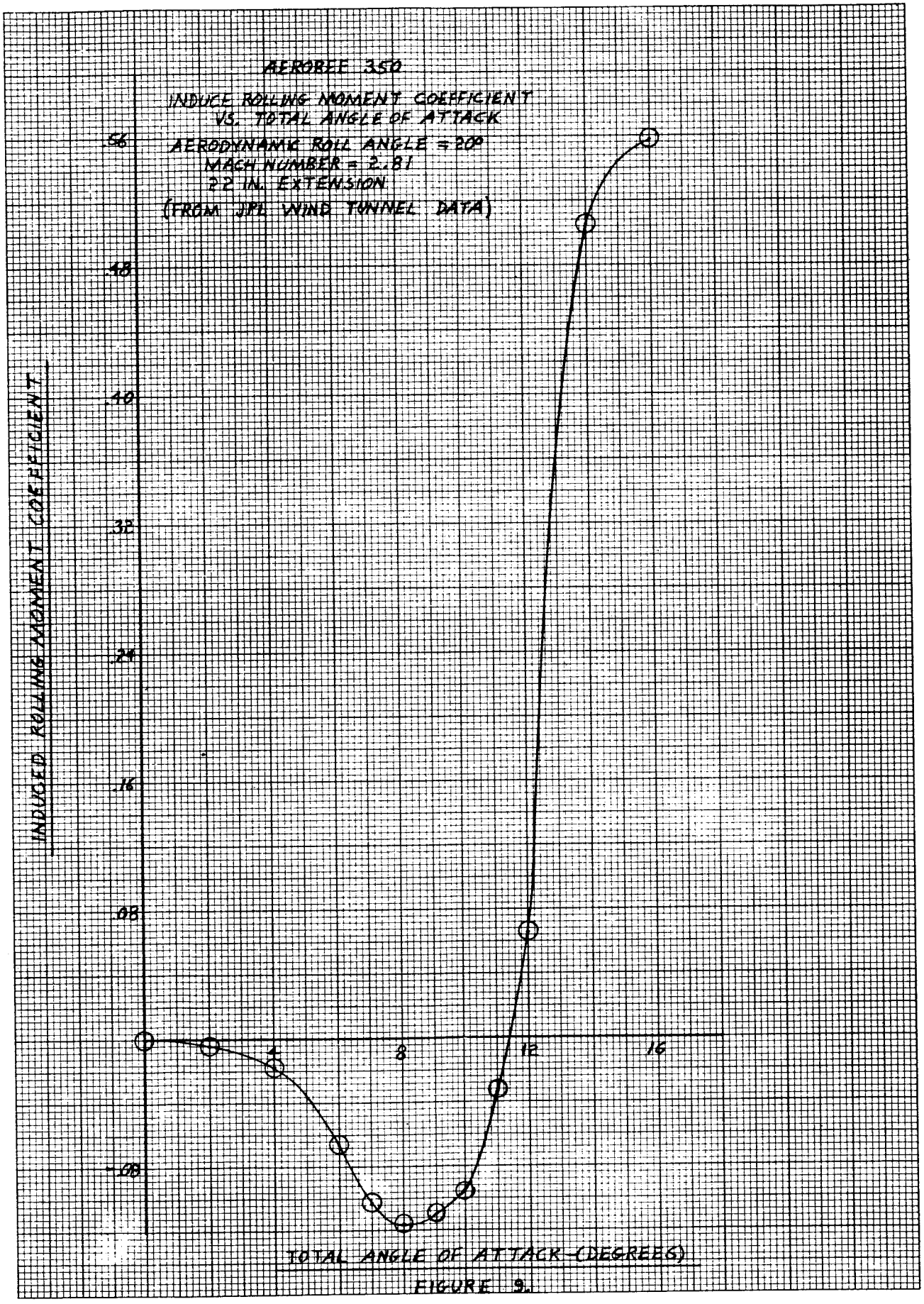
AEROBEE 350
INDUCE ROLLING MOMENT COEFFICIENT VS. TOTAL ANGLE OF ATTACK
AERODYNAMIC ROLL ANGLE = 20°
MACH NUMBER = 2.81
22 IN. EXTENSION
(FROM JPL WIND TUNNEL DATA)
.56
.48
.40
.32
.24
.16
.08
-.08
INDUCED ROLLING MOMENT COEFFICIENT
4
8
12
16
TOTAL ANGLE OF ATTACK (DEGREES)

FIGURE 9.

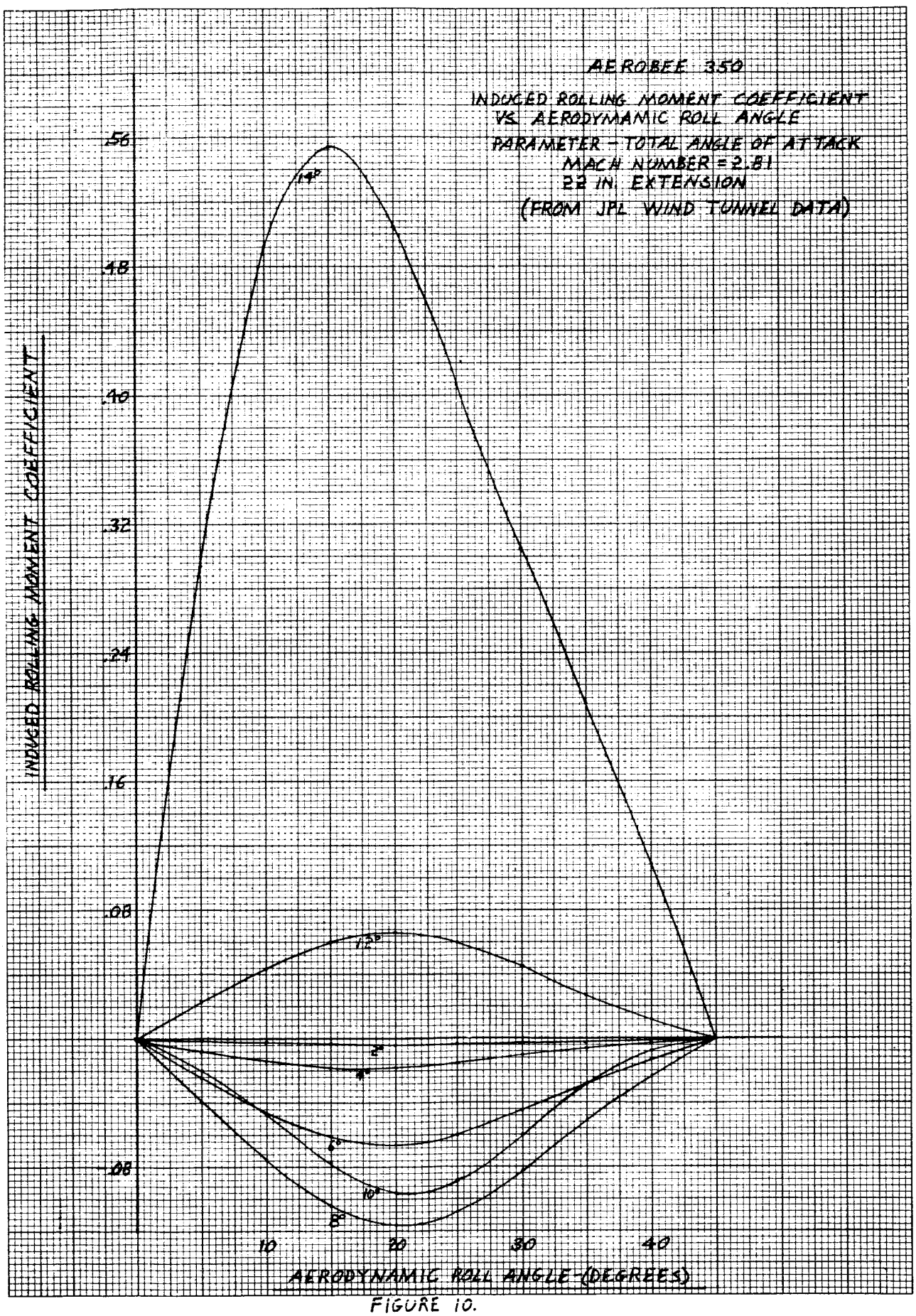
AEROBEE 350
INDUCED ROLLING MOMENT COEFFICIENT VS. AERODYNAMIC ROLL ANGLE
PARAMETER - TOTAL ANGLE OF ATTACK
MACH NUMBER = 2.81
22 IN. EXTENSION
(FROM JPL WIND TUNNEL DATA)
INDUCED ROLLING MOMENT COEFFICIENT
.56
.48
.40
.32
.24
.16
.08
-.08
14°
12°
2°
4°
6°
10°
8°
10
20
30
40
AERODYNAMIC ROLL ANGLE - (DEGREES)

FIGURE 10.

AEROBEE 350

SIDE FORCE COEFFICIENT VS.
AERODYNAMIC ROLL ANGLE
PARAMETER- TOTAL ANGLE OF ATTACK
MACH NUMBER = 2.81
22 IN. EXTENSION
(FROM JPL WIND TUNNEL DATA)

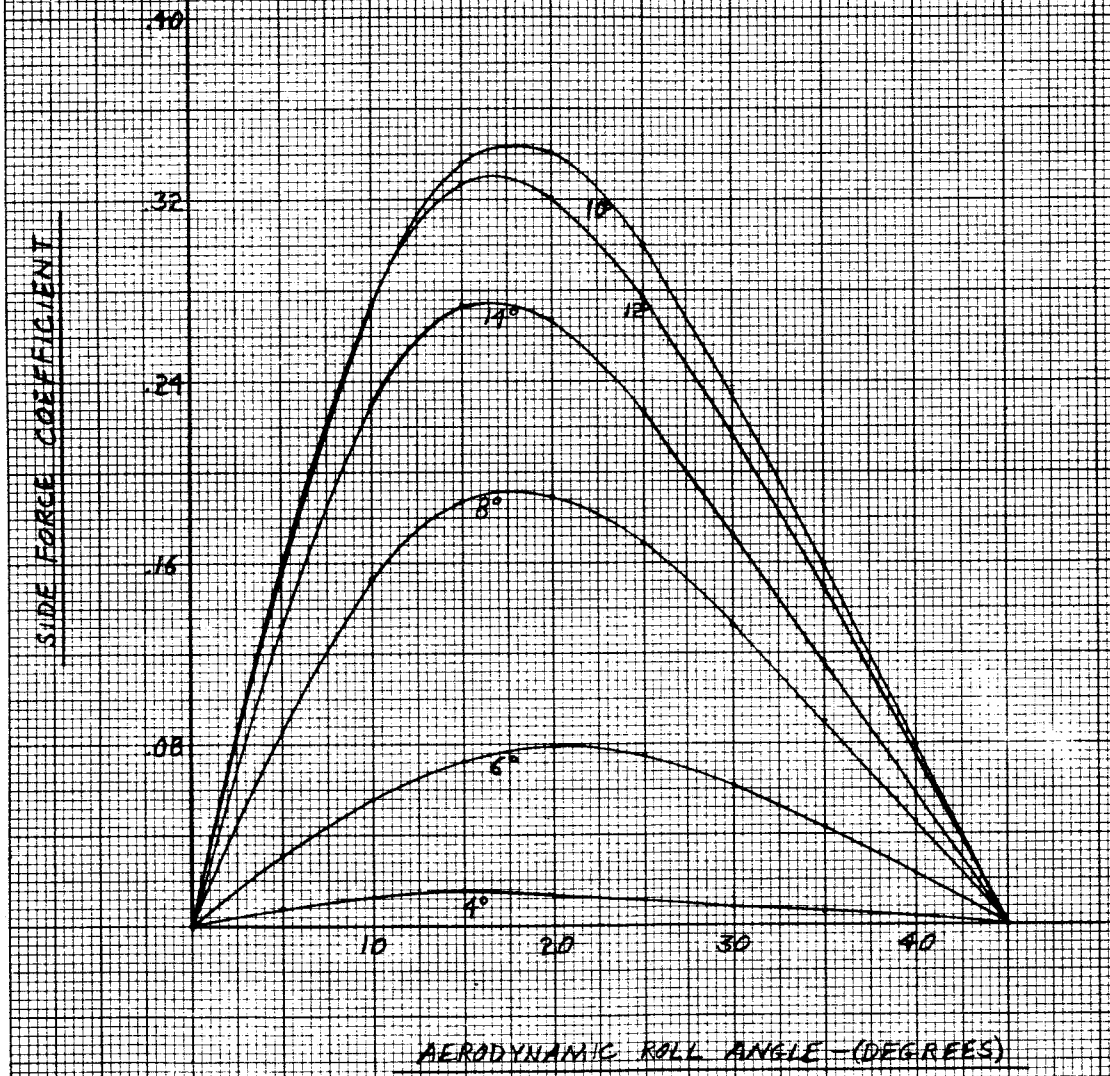

FIGURE 11.

TREND OF THE INDUCED ROLLING MOMENT AS A FUNCTION OF AERODYNAMIC ROLL ANGLE AT LOW TOTAL ANGLES OF ATTACK.

AEROBEE 150A AND AEROBEE 350

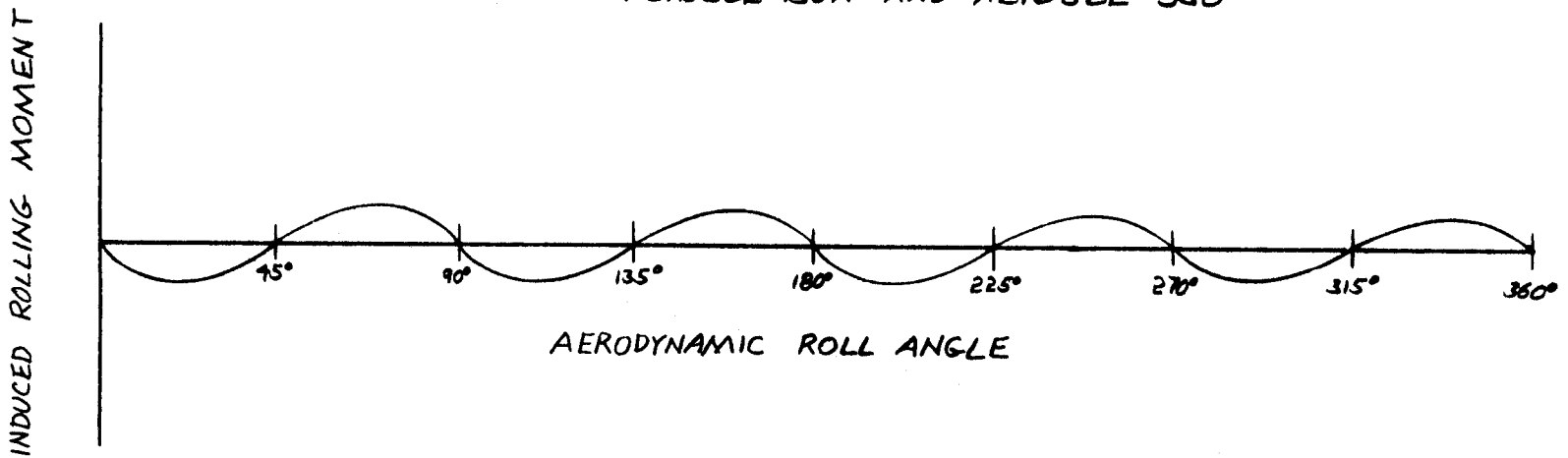

FIGURE 12.

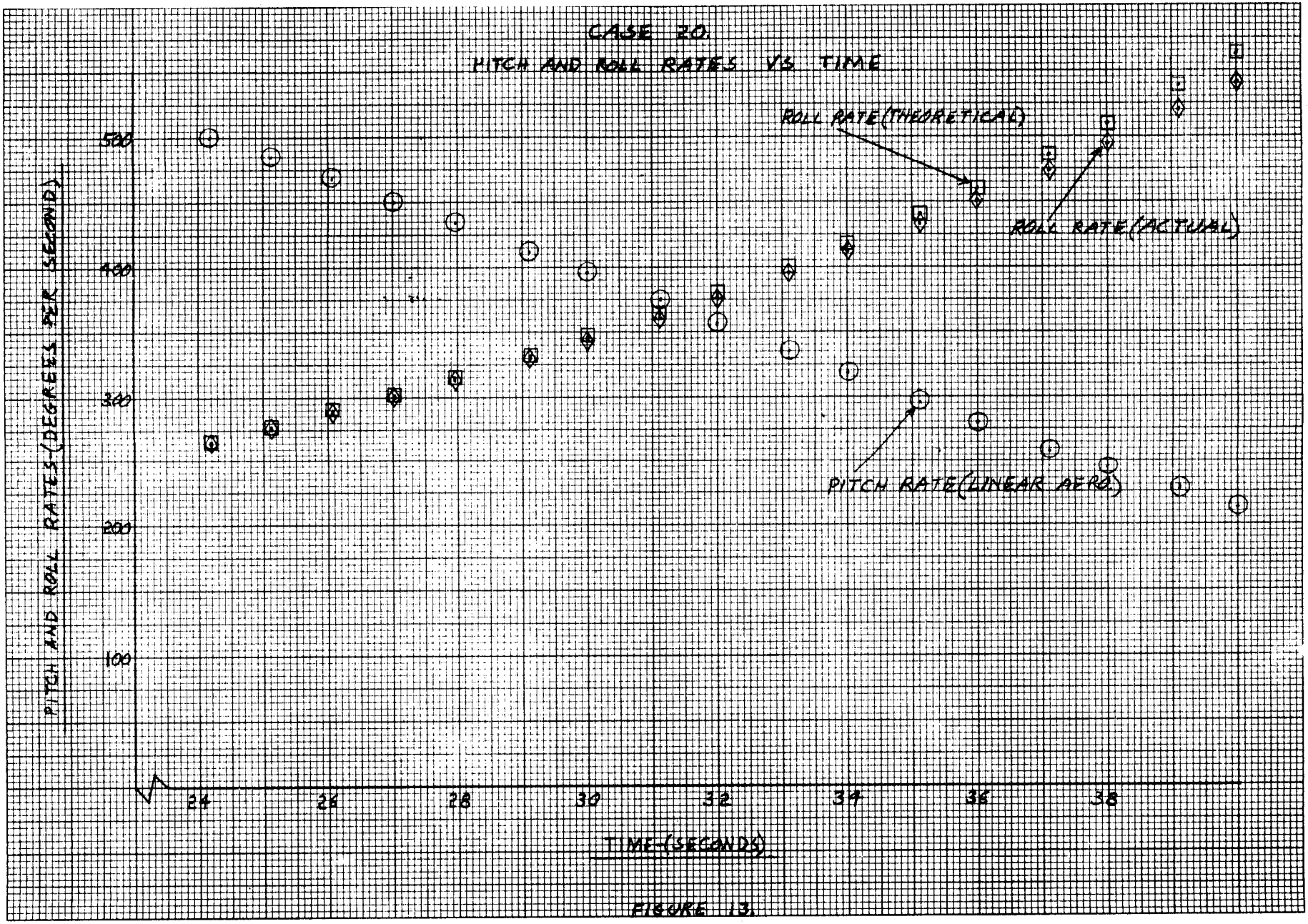
CASE 20.
PITCH AND ROLL RATES VS TIME
ROLL RATE (THEORETICAL)
ROLL RATE (ACTUAL)
PITCH RATE (LINEAR AERO)
PITCH AND ROLL RATES (DEGREES PER SECOND)
500
400
300
200
100
24
26
28
30
32
34
36
38
TIME (SECONDS)

FIGURE 13.

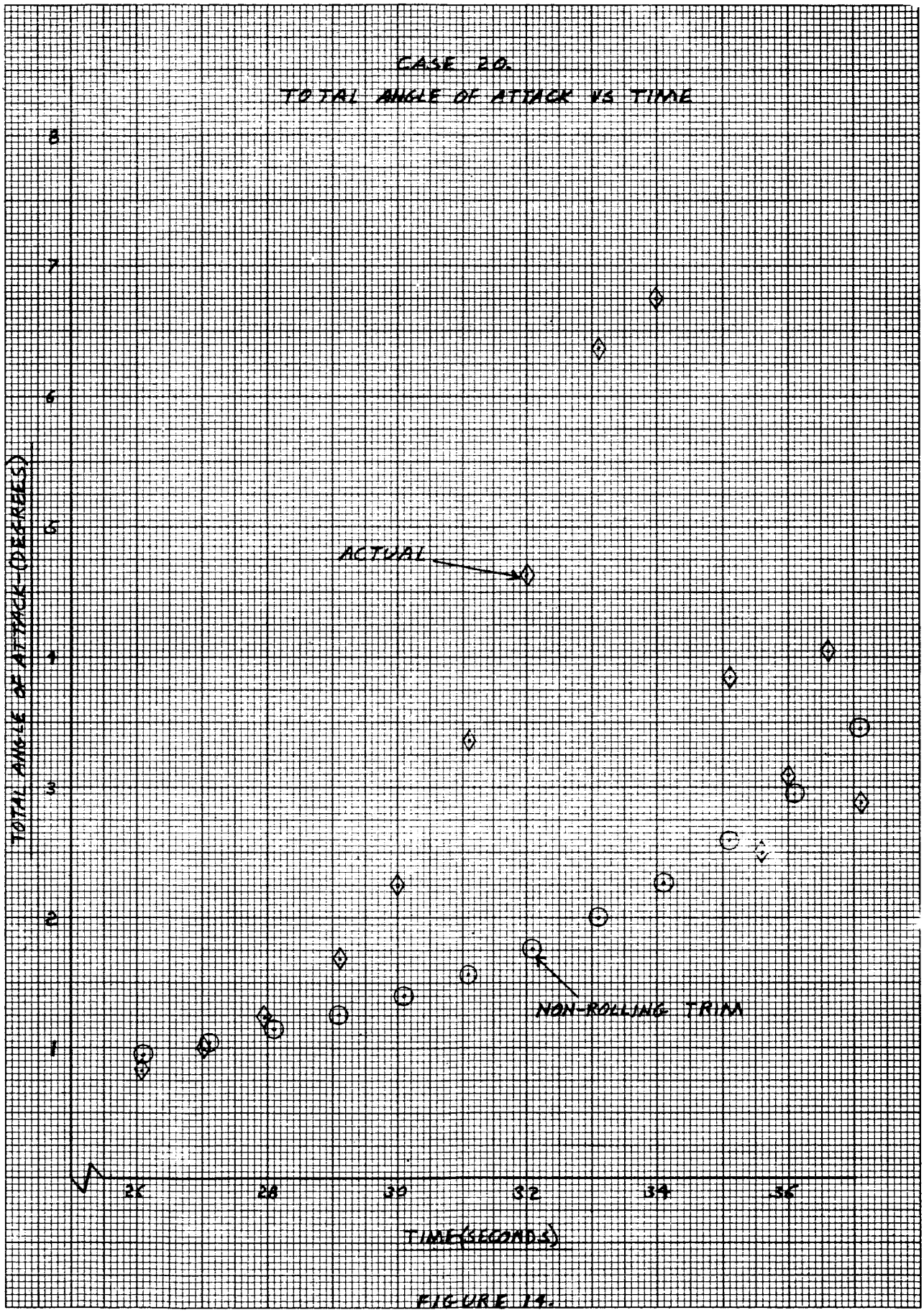
CASE 20.
TOTAL ANGLE OF ATTACK VS TIME
TOTAL ANGLE OF ATTACK-(DEGREES)
8
7
6
5
4
3
2
1
ACTUAL
NON-ROLLING TRIM
26
30
32
34
36
TIME(SECONDS)

FIGURE 14.

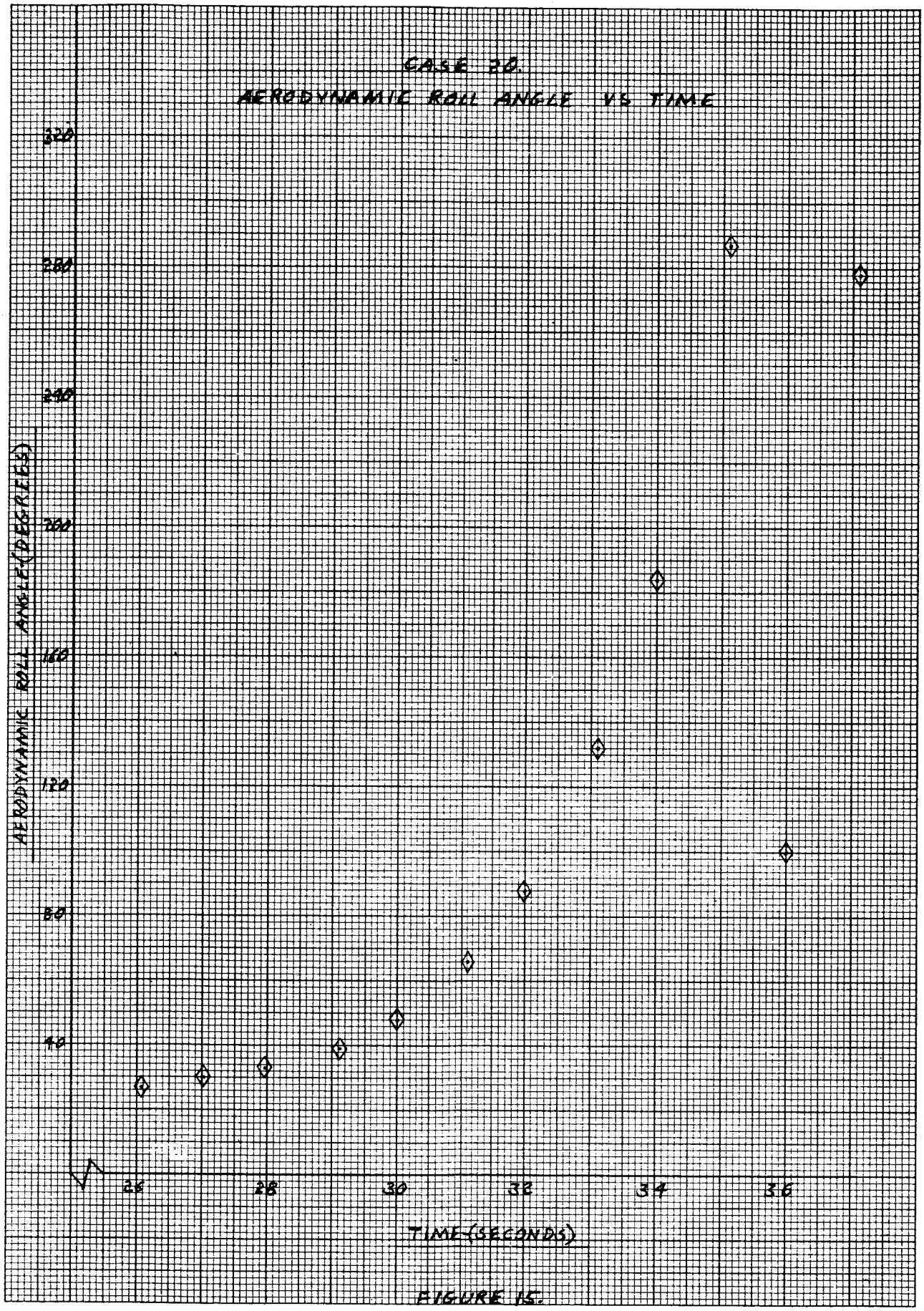
CASE 20.
AERODYNAMIC ROLL ANGLE VS TIME
320
280
240
200
160
120
80
40
AERODYNAMIC ROLL ANGLE (DEGREES)
26
28
30
32
34
36
TIME (SECONDS)

FIGURE 15.

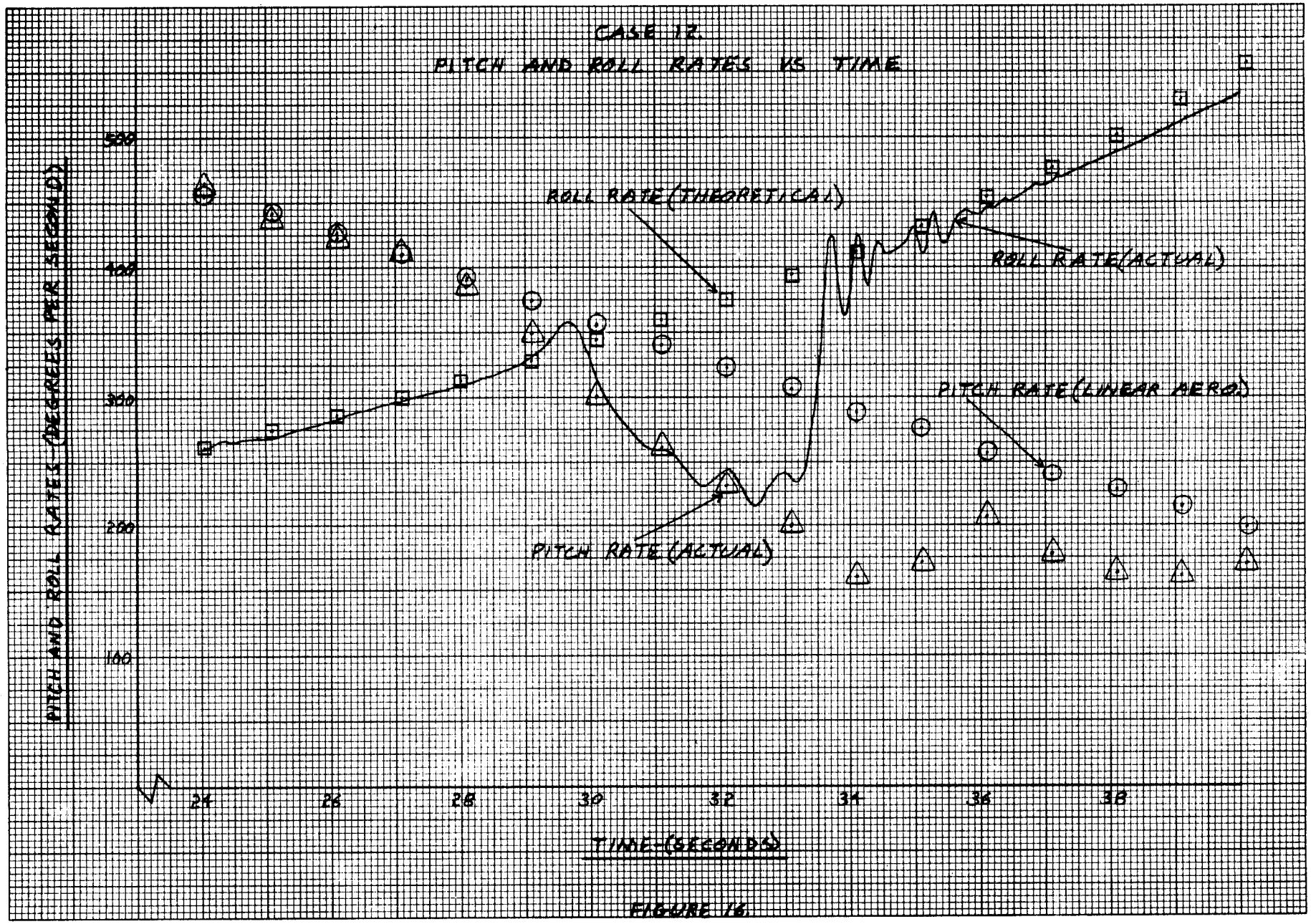
CASE 12.
PITCH AND ROLL RATES VS TIME
ROLL RATE (THEORETICAL)
ROLL RATE (ACTUAL)
PITCH RATE (LINEAR AERO)
PITCH RATE (ACTUAL)
PITCH AND ROLL RATES - (DEGREES PER SECOND)
500
400
300
200
100
24
26
28
30
32
34
36
38
TIME - (SECONDS)

FIGURE 16

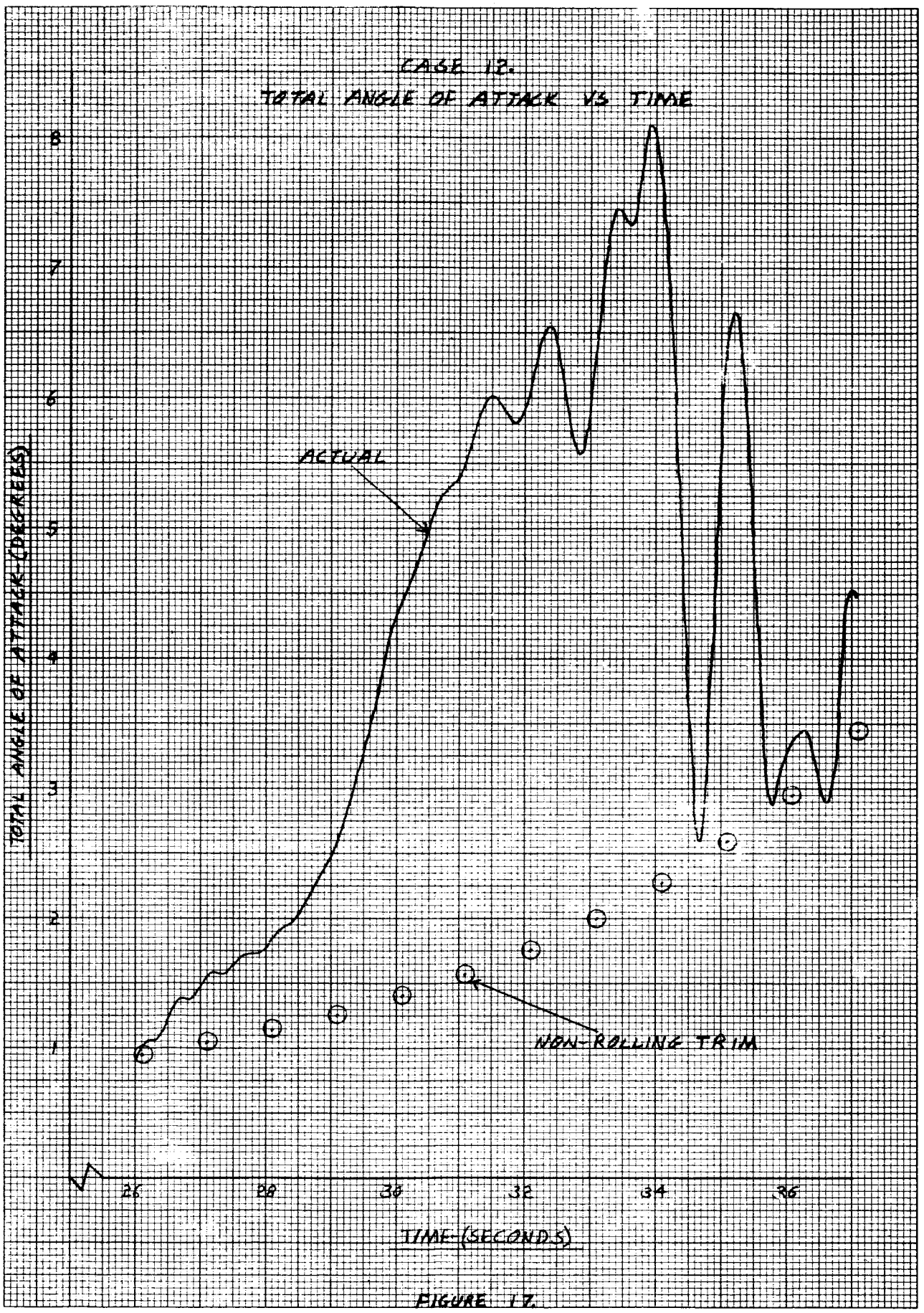
CASE 12.
TOTAL ANGLE OF ATTACK VS TIME
TOTAL ANGLE OF ATTACK (DEGREES)
8
7
6
5
4
3
2
1
ACTUAL
NON-ROLLING TRIM
26
28
30
32
34
36
TIME-(SECONDS)

FIGURE 17.

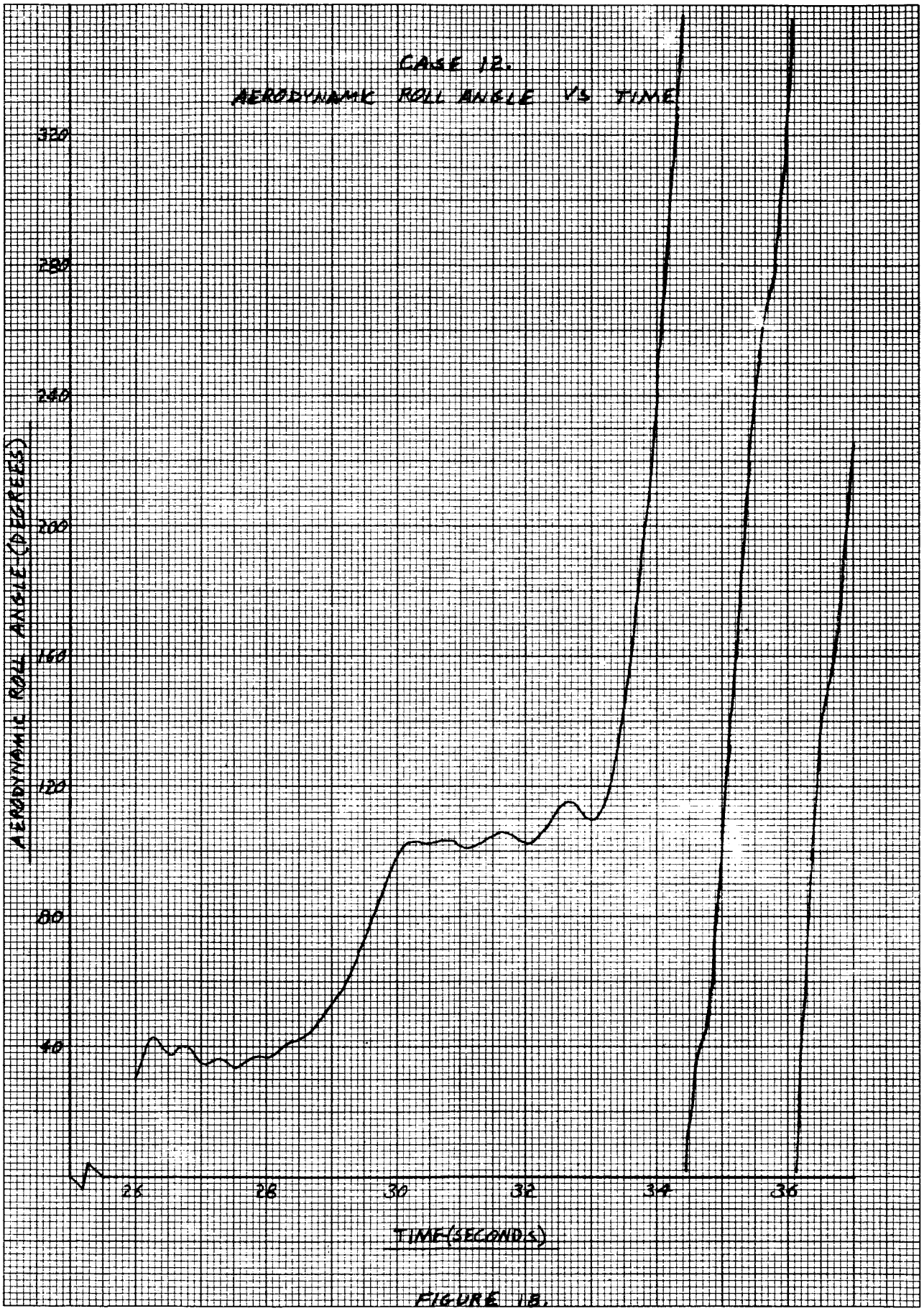
CASE 12.
AERODYNAMIC ROLL ANGLE VS TIME
320
280
240
200
160
120
80
40
AERODYNAMIC ROLL ANGLE-(DEGREES)
26
28
30
32
34
36
TIME(SECONDS)

FIGURE 18.

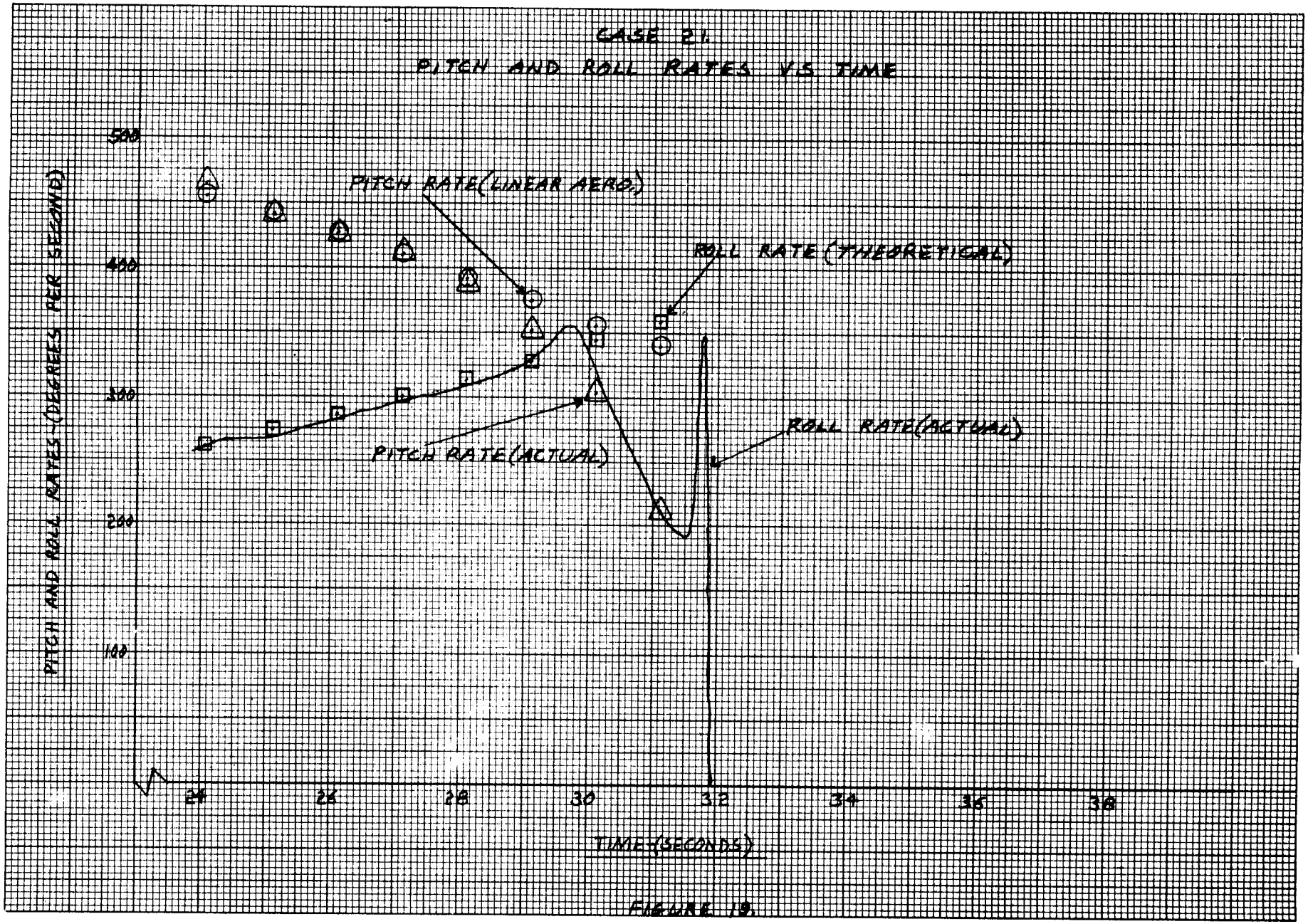
CASE 21
PITCH AND ROLL RATES VS. TIME
PITCH RATE(LINEAR AERO)
ROLL RATE (THEORETICAL)
PITCH RATE(ACTUAL)
ROLL RATE(ACTUAL)
PITCH AND ROLL RATES (DEGREES PER SECOND)
500
400
300
200
100
24
26
28
30
32
34
36
38
TIME (SECONDS)

FIGURE 19.

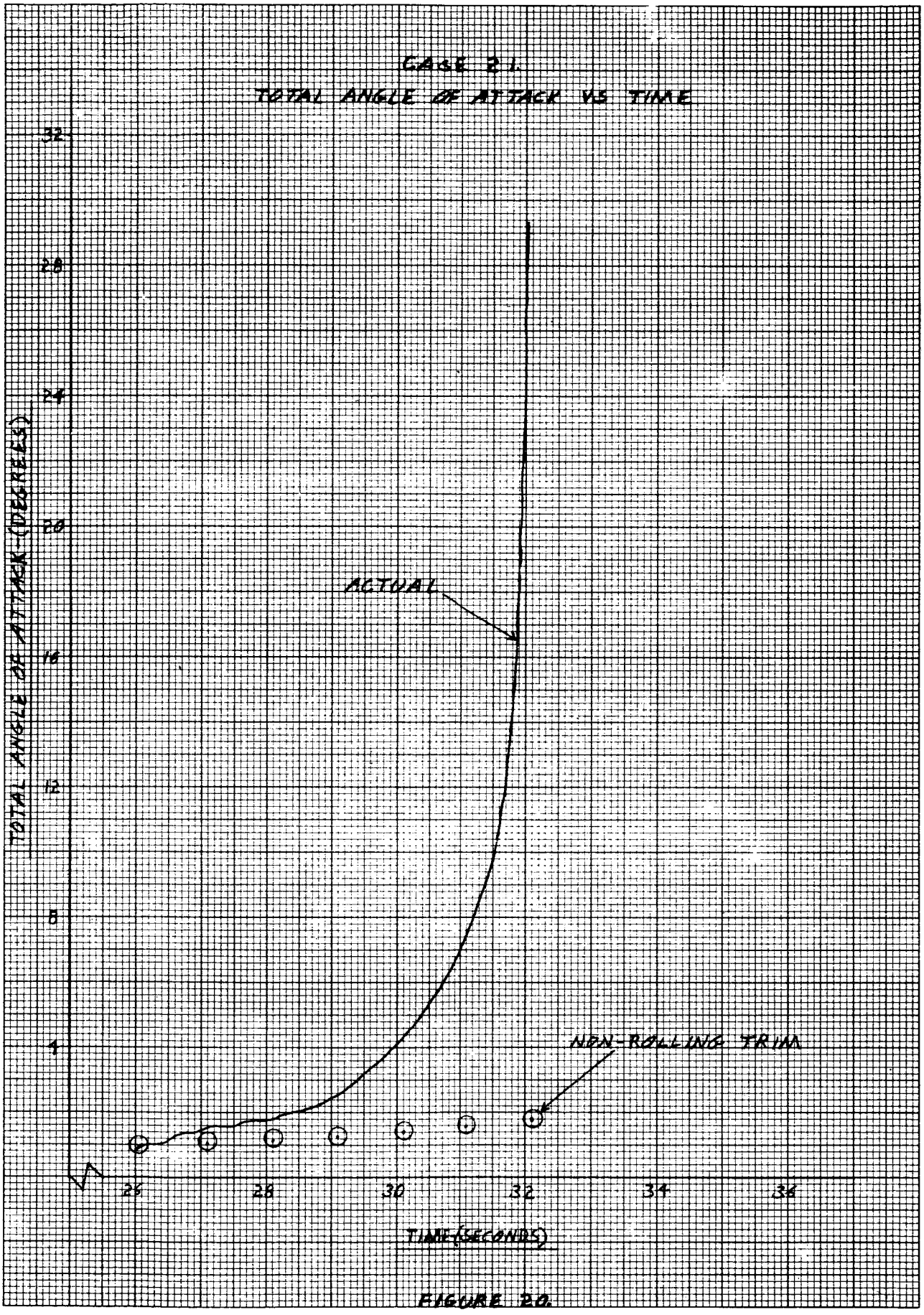
CASE 2.1.
TOTAL ANGLE OF ATTACK VS TIME
32
28
24
20
16
12
8
4
TOTAL ANGLE OF ATTACK-(DEGREES)
ACTUAL
NON-ROLLING TRIM
26
28
30
32
34
36
TIME (SECONDS)

FIGURE 20.

CASE 21.

AERODYNAMIC ROLL ANGLE VS TIME

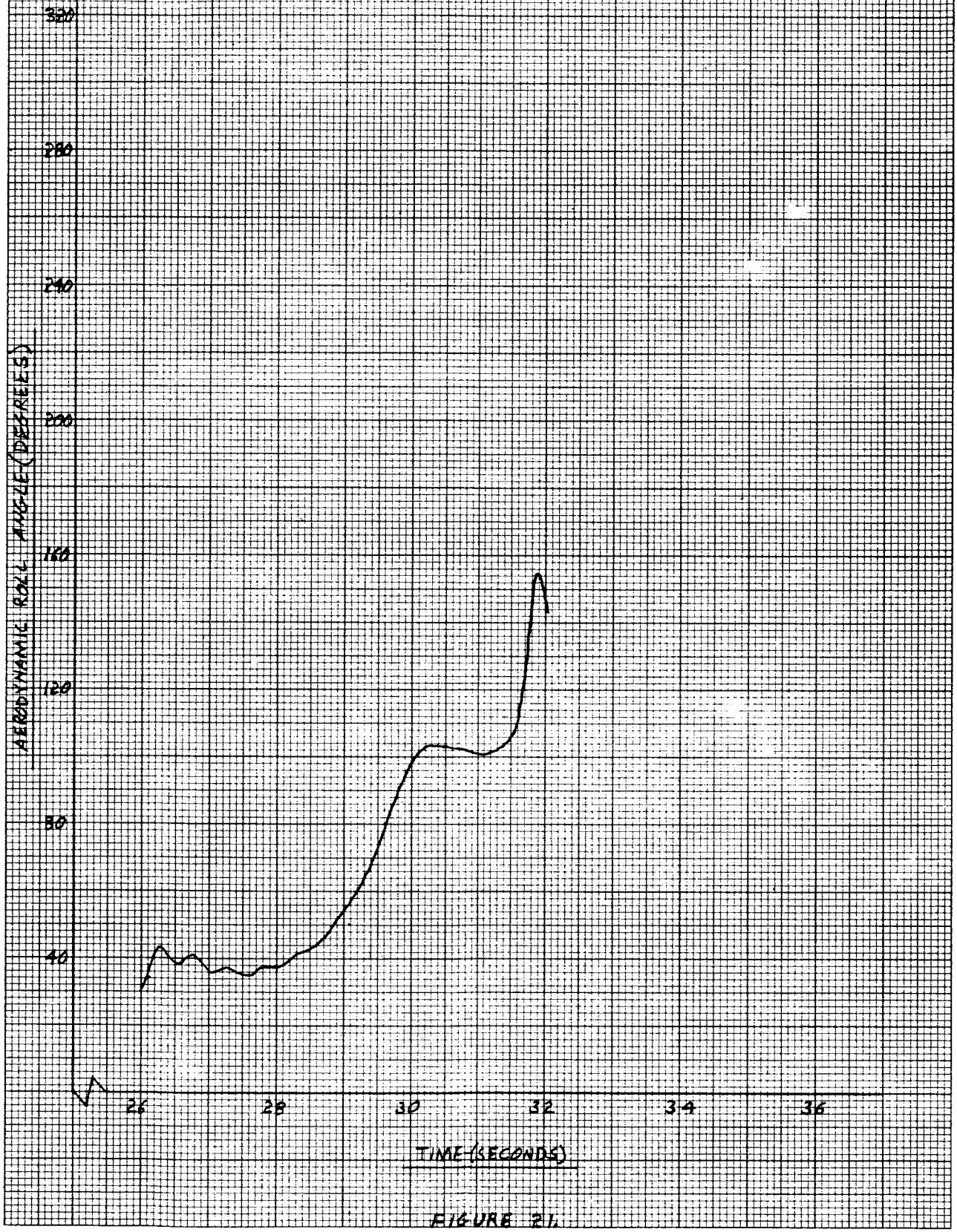

FIGURE 21

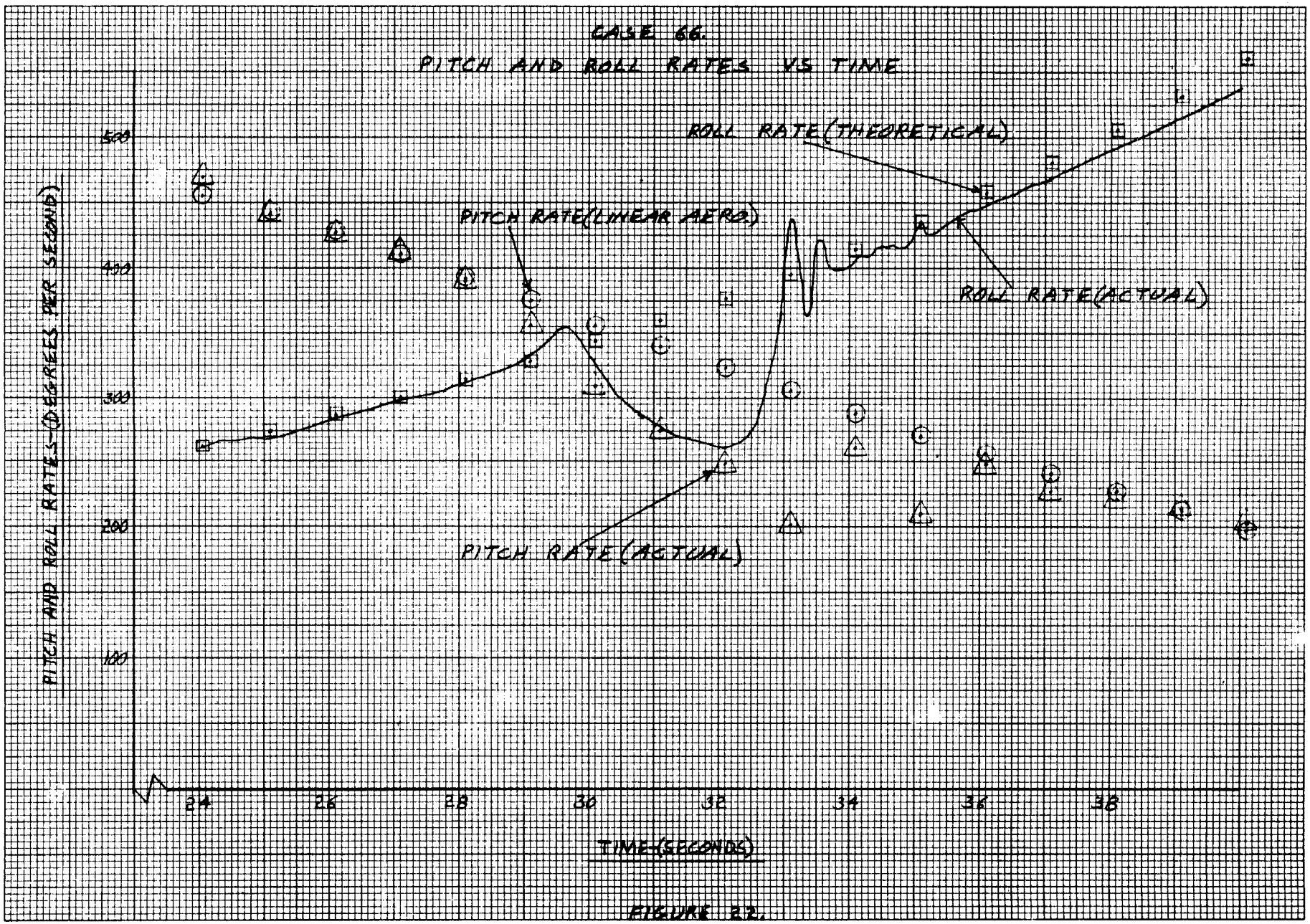
CASE 66.
PITCH AND ROLL RATES VS TIME
ROLL RATE (THEORETICAL)
PITCH RATE (LINEAR AERO)
ROLL RATE (ACTUAL)
PITCH RATE (ACTUAL)
PITCH AND ROLL RATES - (DEGREES PER SECOND)
500
400
300
200
100
24
26
28
30
32
34
36
38
TIME - (SECONDS)

FIGURE 22.

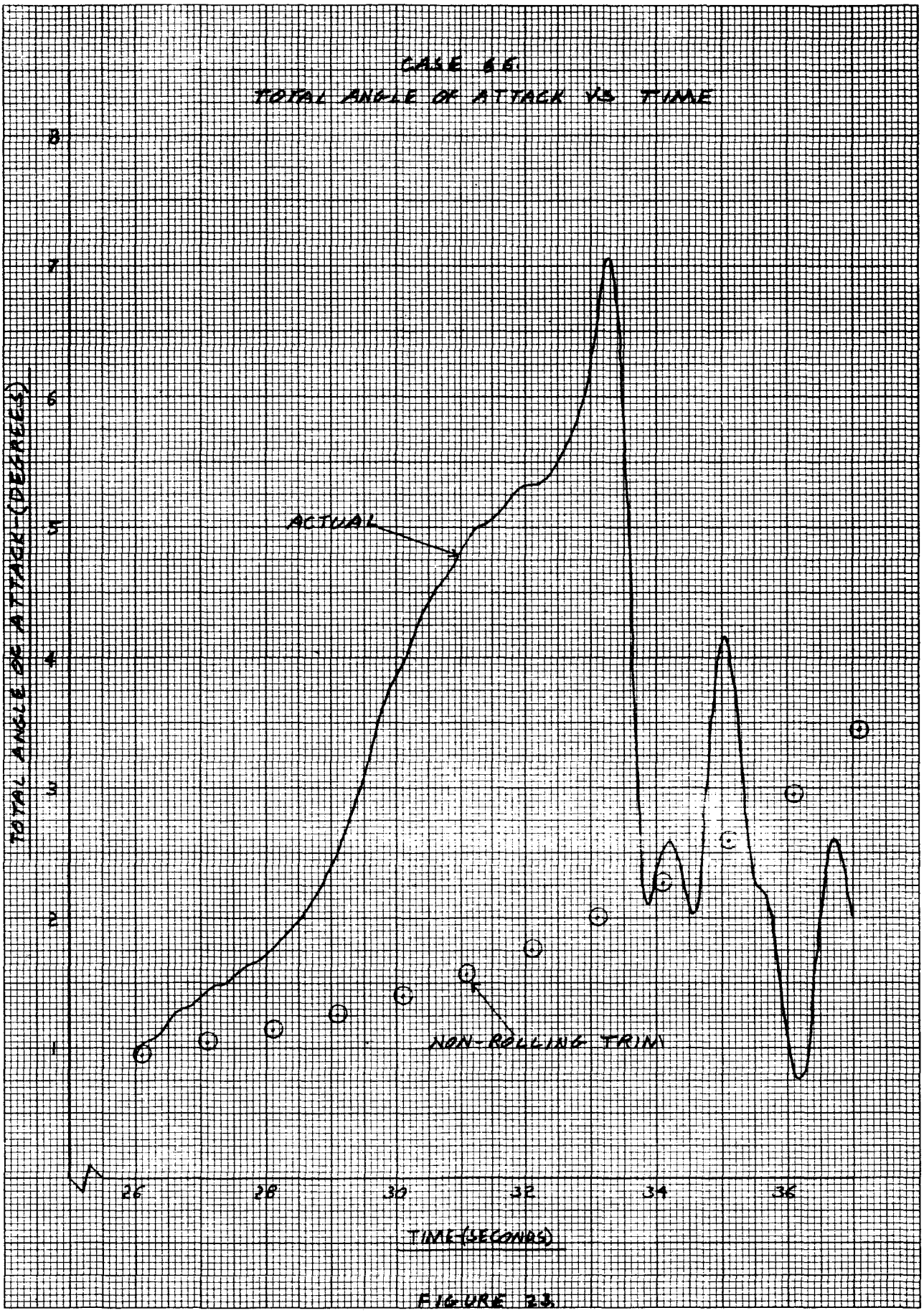
CASE 66
TOTAL ANGLE OF ATTACK VS TIME
TOTAL ANGLE OF ATTACK-(DEGREES)
8
7
6
5
4
3
2
1
ACTUAL
NON-ROLLING TRIM
26
28
30
32
34
36
TIME-(SECONDS)

FIGURE 23.

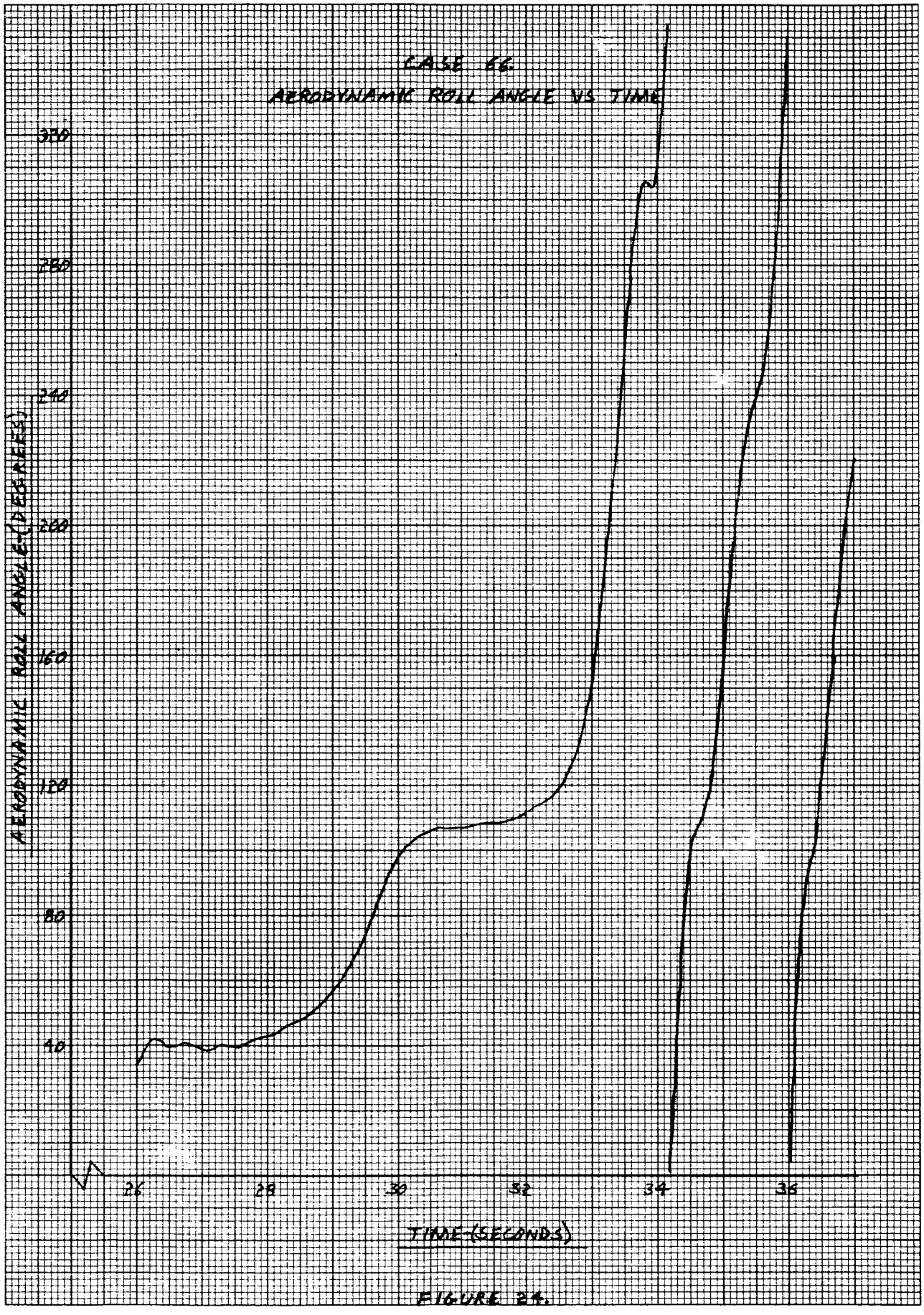
CASE 66.
AERODYNAMIC ROLL ANGLE VS TIME
AERODYNAMIC ROLL ANGLE-(DEGREES)
360
280
240
200
160
120
80
40
26
28
30
32
34
36
TIME-(SECONDS)

FIGURE 24.

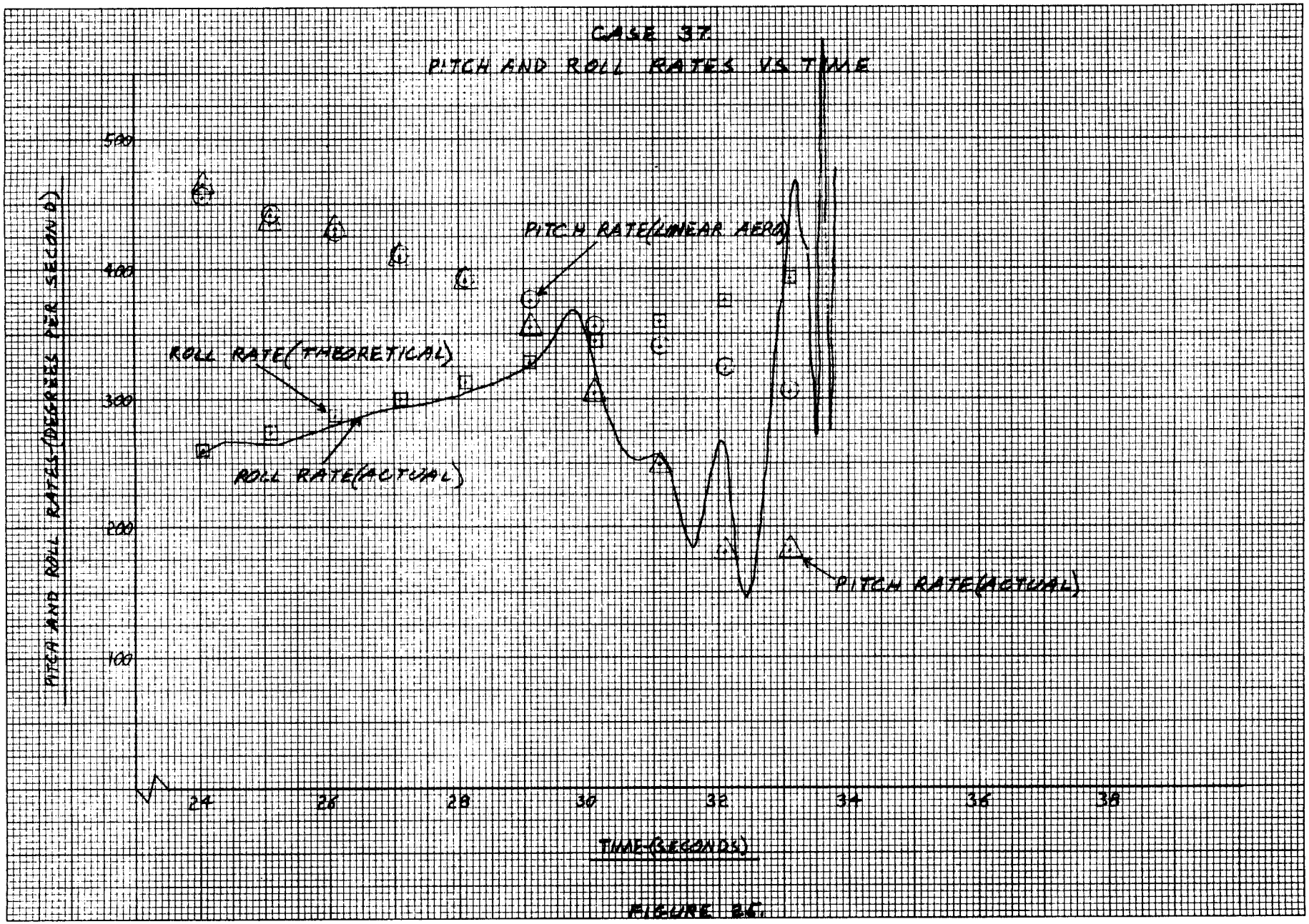
CASE 37
PITCH AND ROLL RATES VS TIME
PITCH AND ROLL RATES-(DEGREES PER SECOND)
500
400
300
200
100
PITCH RATE(LINEAR AERO)
ROLL RATE(THEORETICAL)
ROLL RATE(ACTUAL)
PITCH RATE(ACTUAL)
24
26
28
30
32
34
36
38
TIME-(SECONDS)

FIGURE 26.

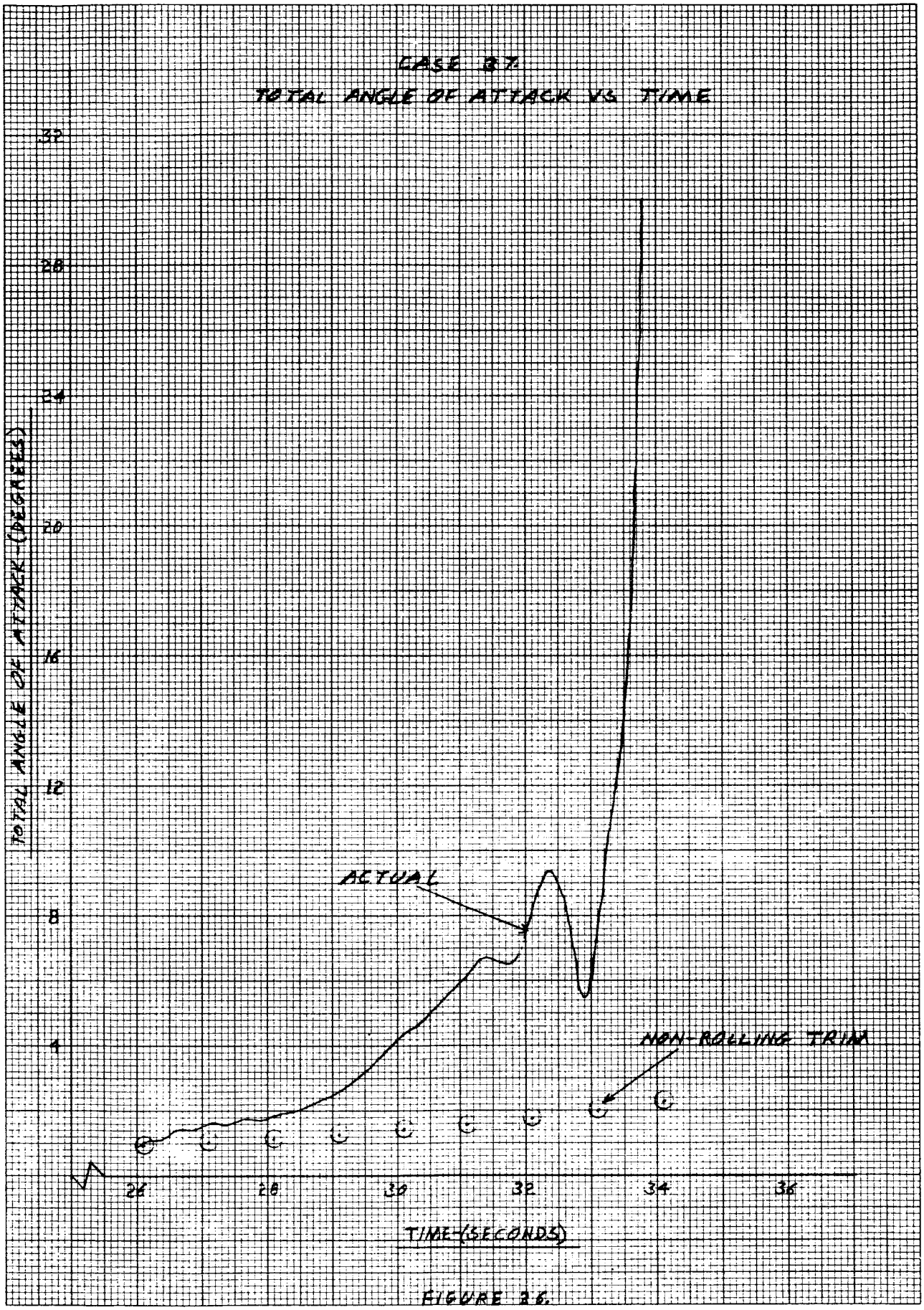
CASE 37
TOTAL ANGLE OF ATTACK VS. TIME
32
28
24
20
16
12
8
4
TOTAL ANGLE OF ATTACK-(DEGREES)
ACTUAL
NON-ROLLING TRIM
26
28
30
32
34
36
TIME-(SECONDS)

FIGURE 26.

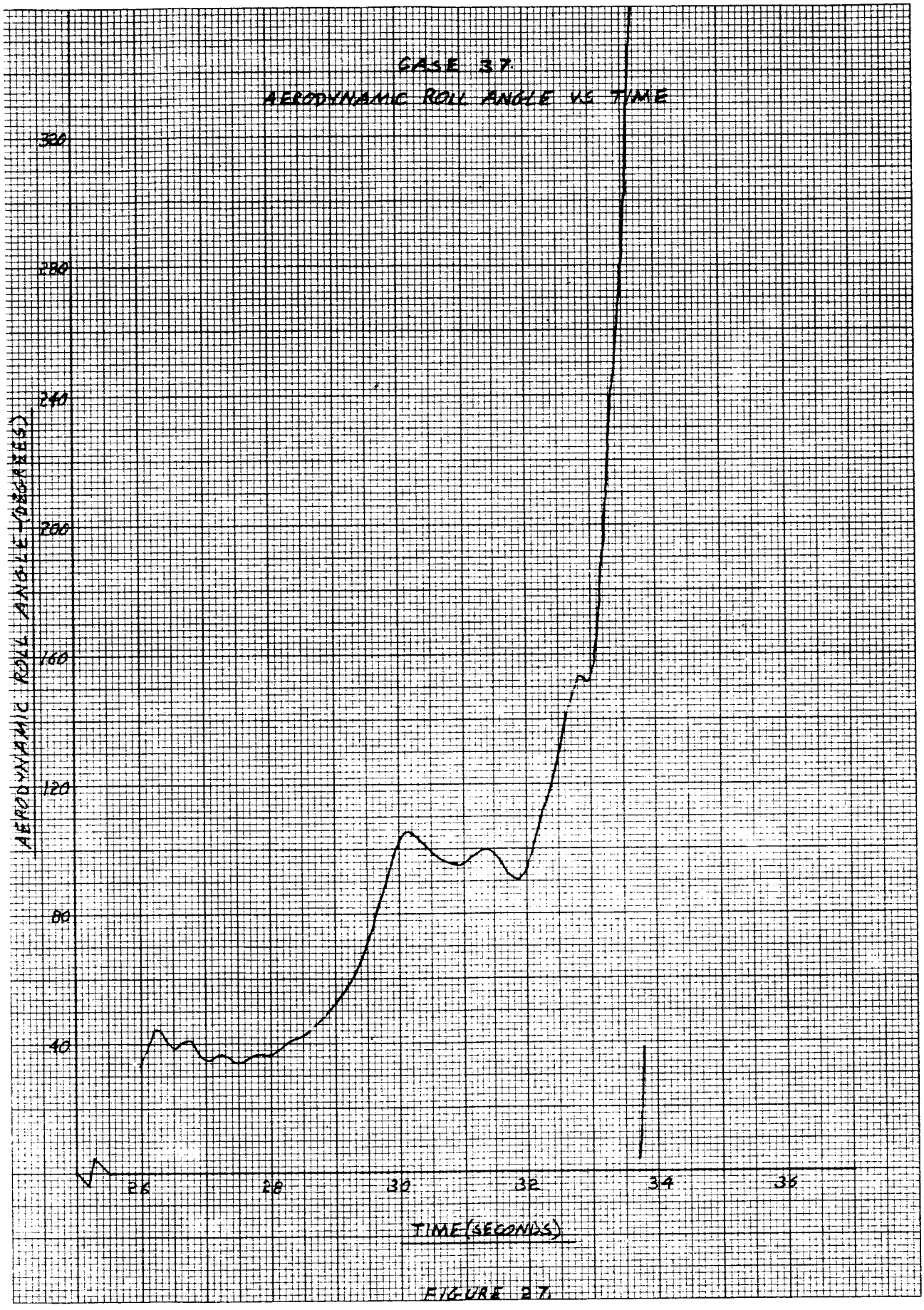
CASE 37
AERODYNAMIC ROLL ANGLE VS TIME
320
280
240
200
160
120
80
40
AERODYNAMIC ROLL ANGLE (DEGREES)
26
28
30
32
34
36
TIME (SECONDS)

FIGURE 27

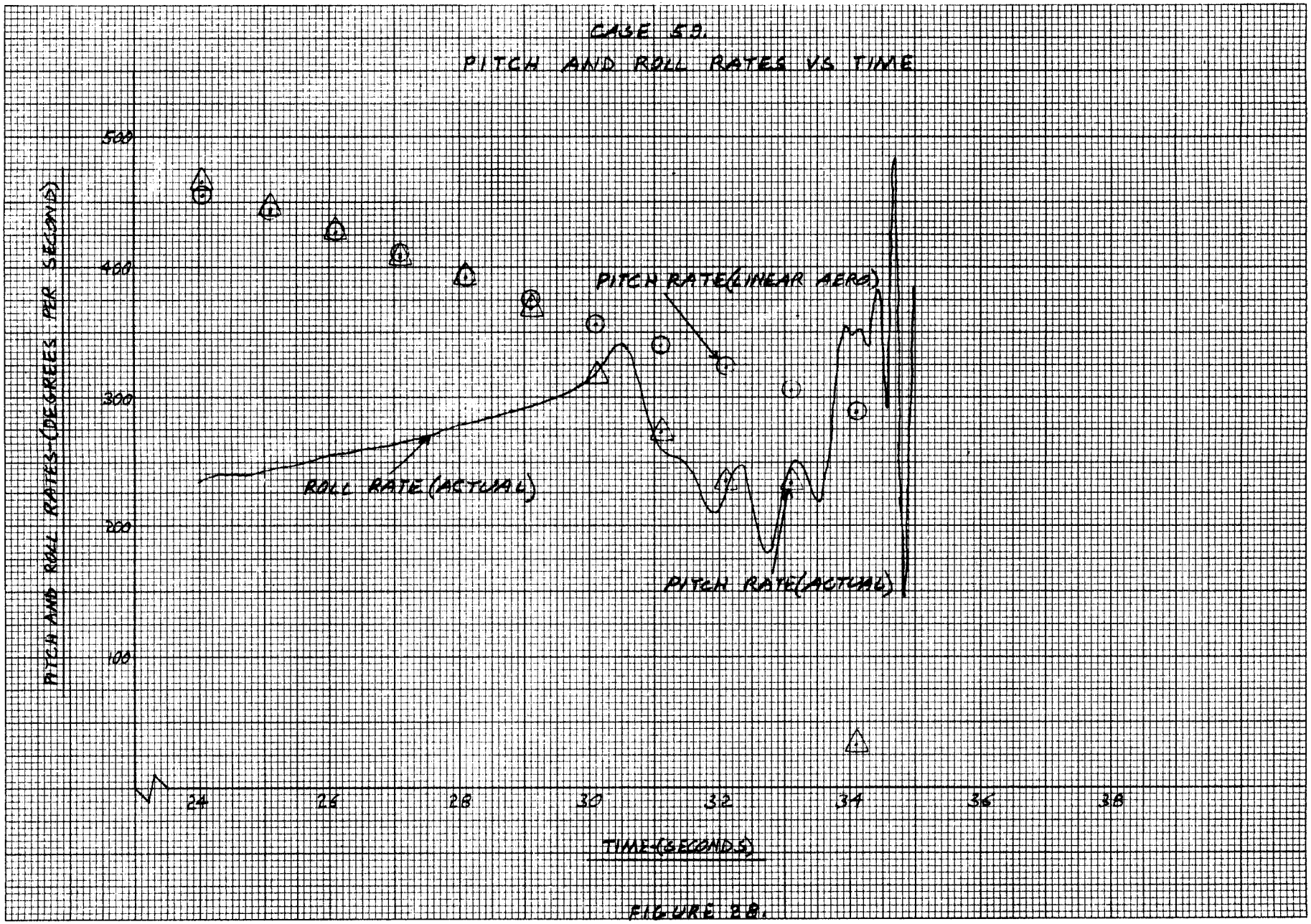
CASE 59.
PITCH AND ROLL RATES VS. TIME
PITCH AND ROLL RATES-(DEGREES PER SECOND)
500
400
300
200
100
PITCH RATE(LINEAR AERO)
ROLL RATE (ACTUAL)
PITCH RATE(ACTUAL)
24
26
28
30
32
34
36
38
TIME-(SECONDS)

FIGURE 28.

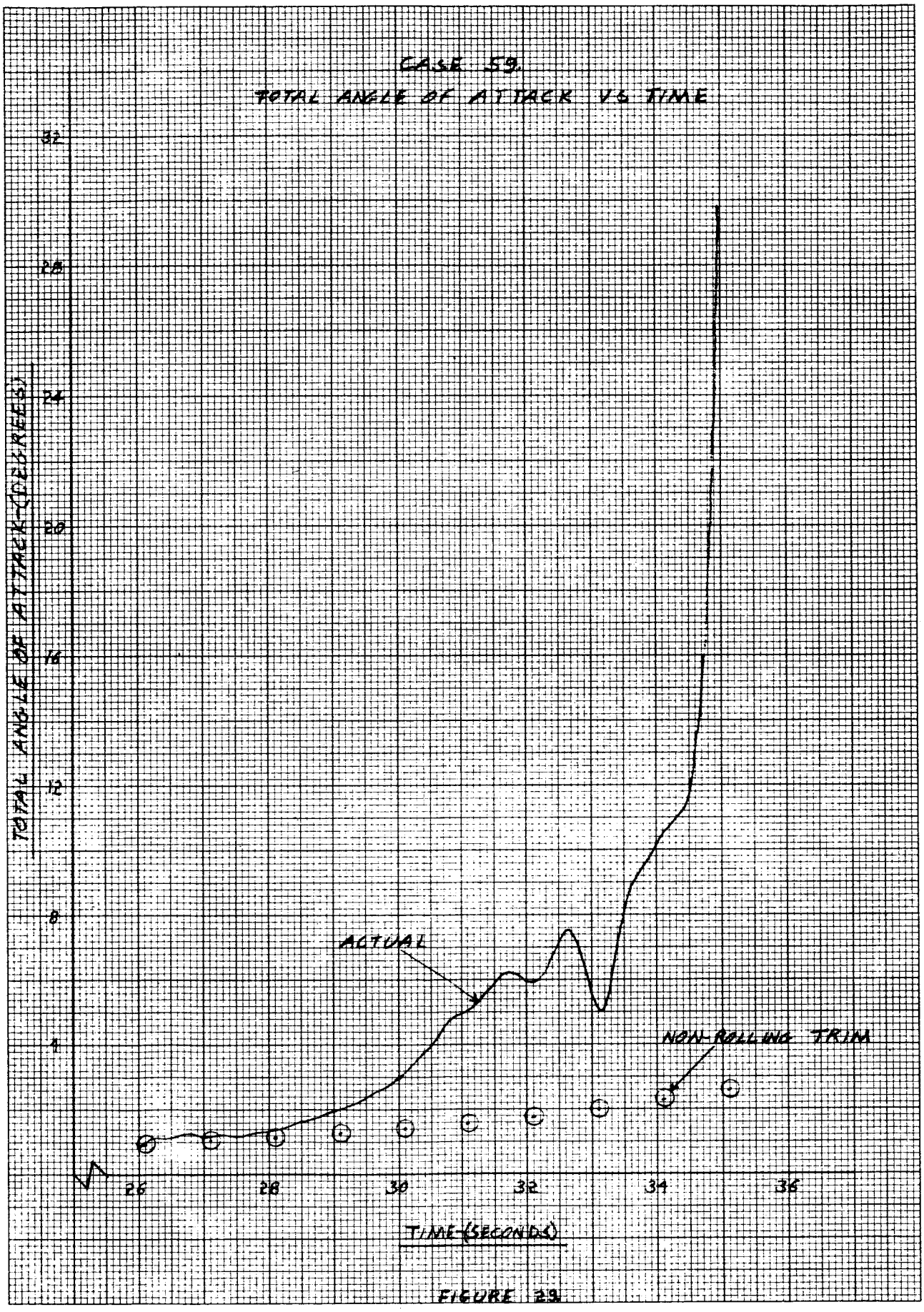
CASE 59.
TOTAL ANGLE OF ATTACK VS TIME
TOTAL ANGLE OF ATTACK-(DEGREES)
32
28
24
20
16
12
8
4
ACTUAL
NON-ROLLING TRIM
26
28
30
32
34
36
TIME-(SECONDS)

FIGURE 29

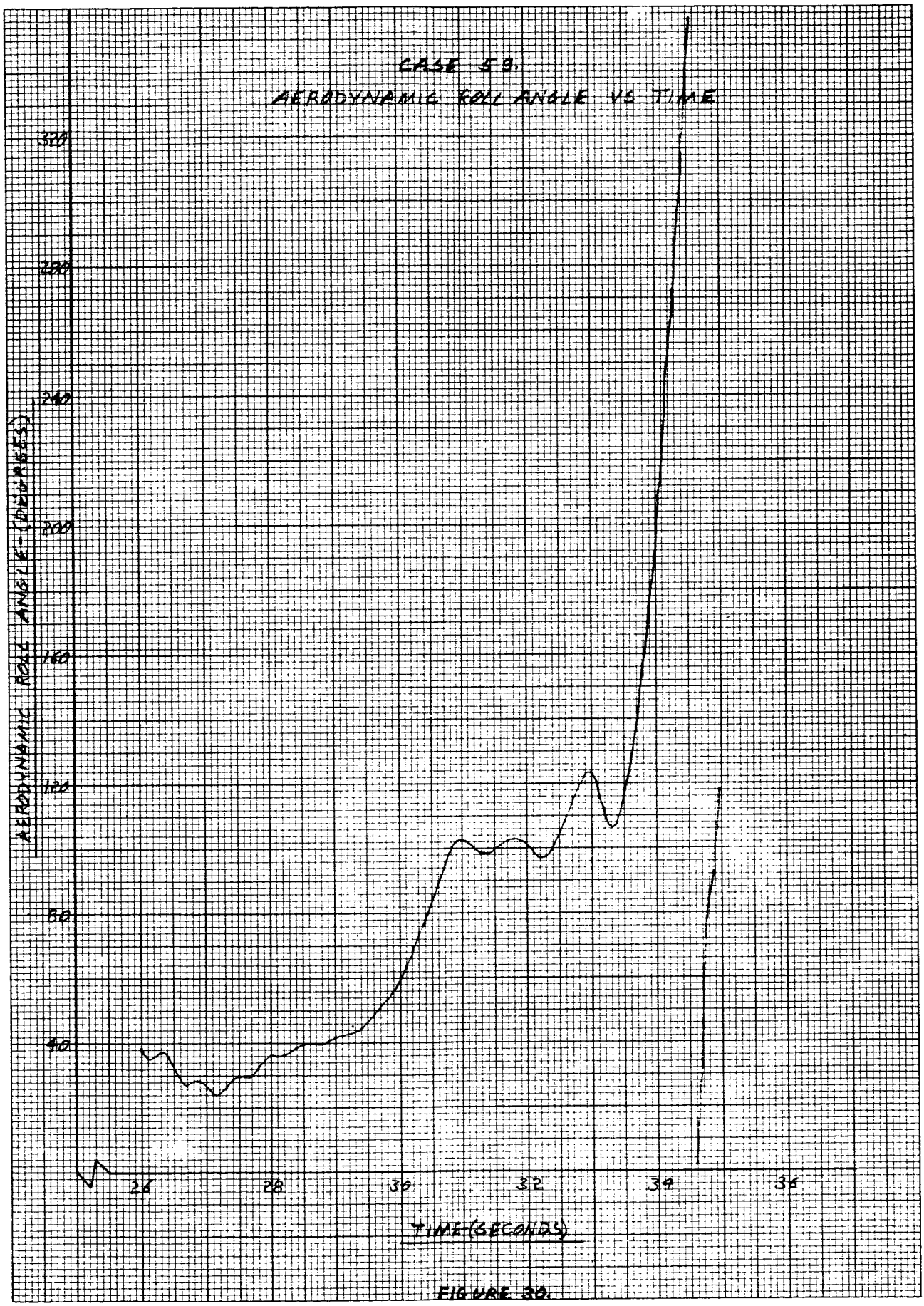
CASE 58.
AERODYNAMIC ROLL ANGLE VS TIME
AERODYNAMIC ROLL ANGLE-(DEGREES)
300
200
240
200
160
120
80
40
26
28
30
32
34
36
TIME-(SECONDS)

FIGURE 30.

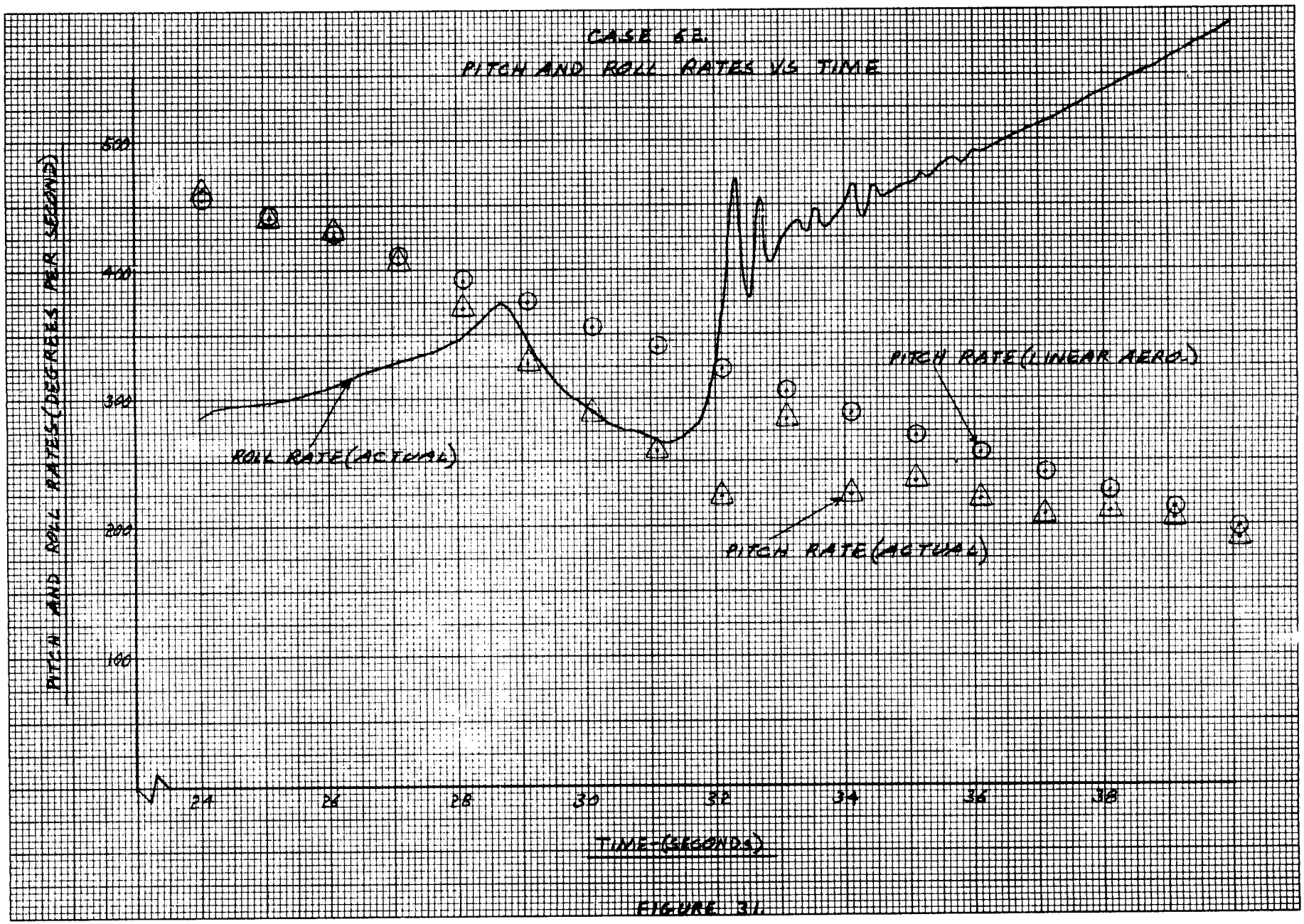
CASE 62.
PITCH AND ROLL RATES VS. TIME
PITCH AND ROLL RATES (DEGREES PER SECOND)
500
400
300
200
100
ROLL RATE (ACTUAL)
PITCH RATE (LINEAR AERO.)
PITCH RATE (ACTUAL)
24
26
28
30
32
34
36
38
TIME - (SECONDS)

FIGURE 31.

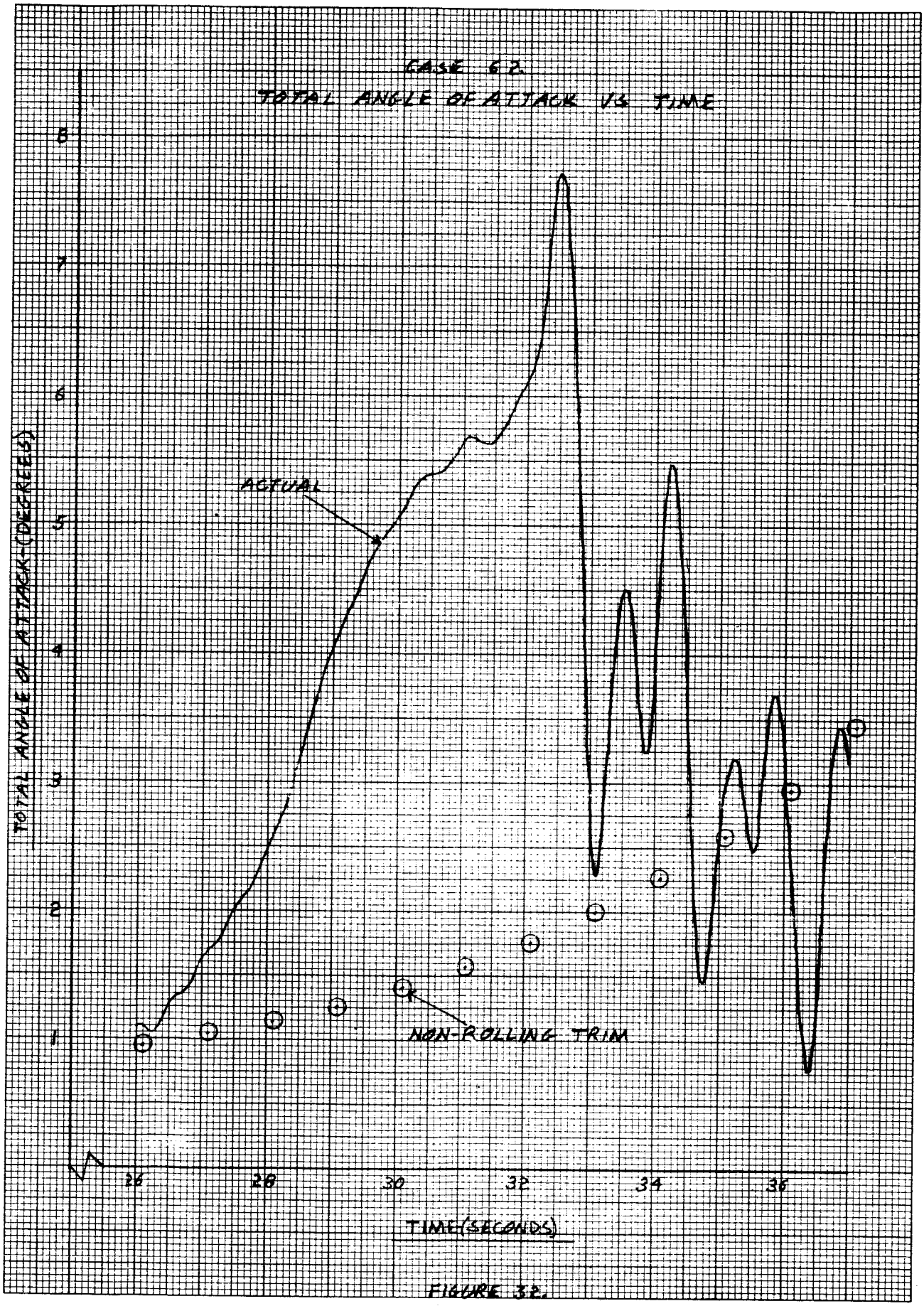
CASE 62.
TOTAL ANGLE OF ATTACK VS TIME
TOTAL ANGLE OF ATTACK (DEGREES)
8
7
6
5
4
3
2
1
ACTUAL
NON-ROLLING TRIM
26
28
30
32
34
36
TIME (SECONDS)

FIGURE 32.

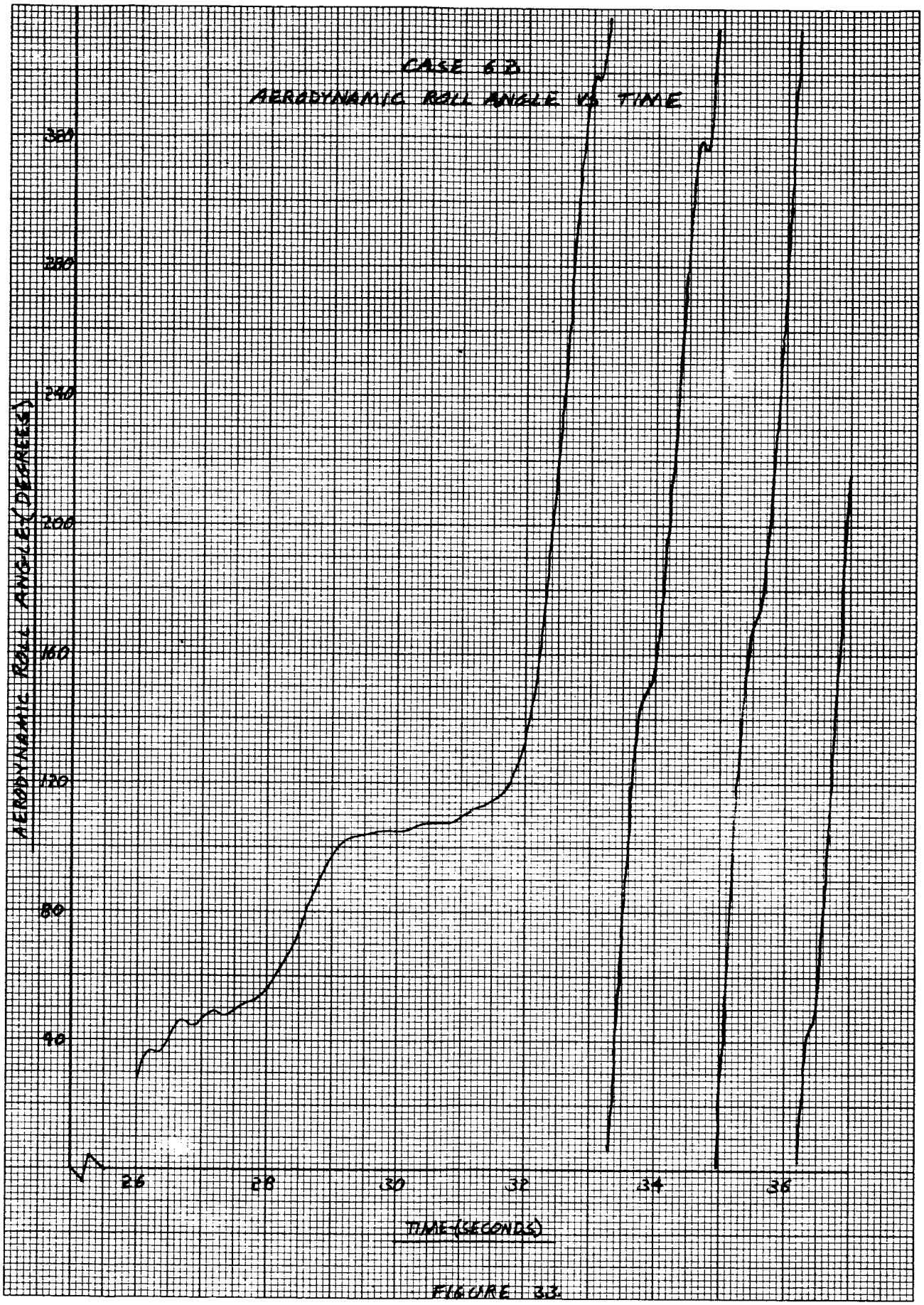
CASE 6 D
AERODYNAMIC ROLL ANGLE VS TIME
AERODYNAMIC ROLL ANGLE (DEGREES)
360
280
240
200
160
120
80
40
26
28
30
32
34
36
TIME (SECONDS)

FIGURE 33

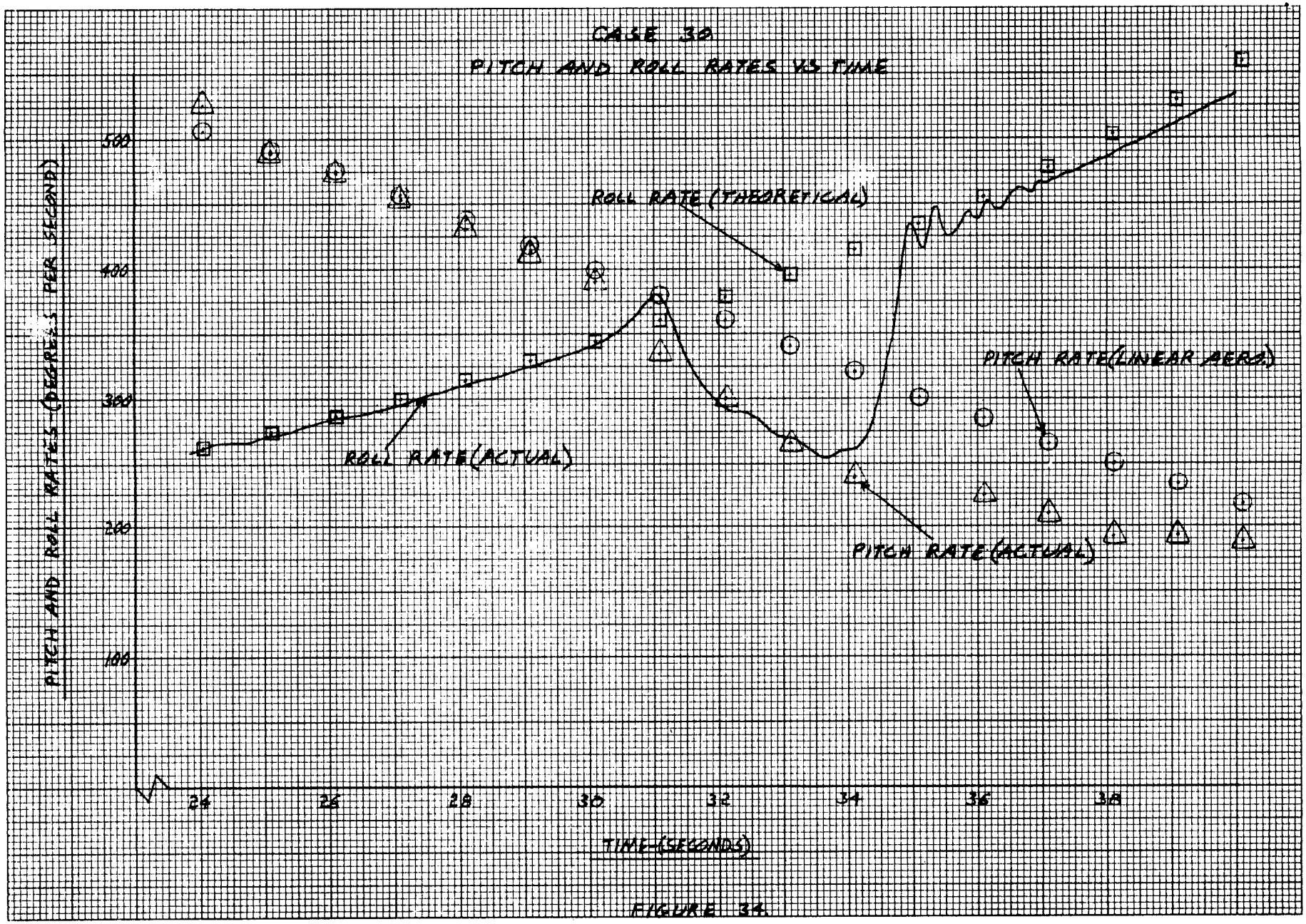
CASE 30
PITCH AND ROLL RATES VS TIME
ROLL RATE (THEORETICAL)
ROLL RATE (ACTUAL)
PITCH RATE (LINEAR AERO)
PITCH RATE (ACTUAL)
PITCH AND ROLL RATES (DEGREES PER SECOND)
500
400
300
200
100
24
26
28
30
32
34
36
38
TIME (SECONDS)

FIGURE 34.

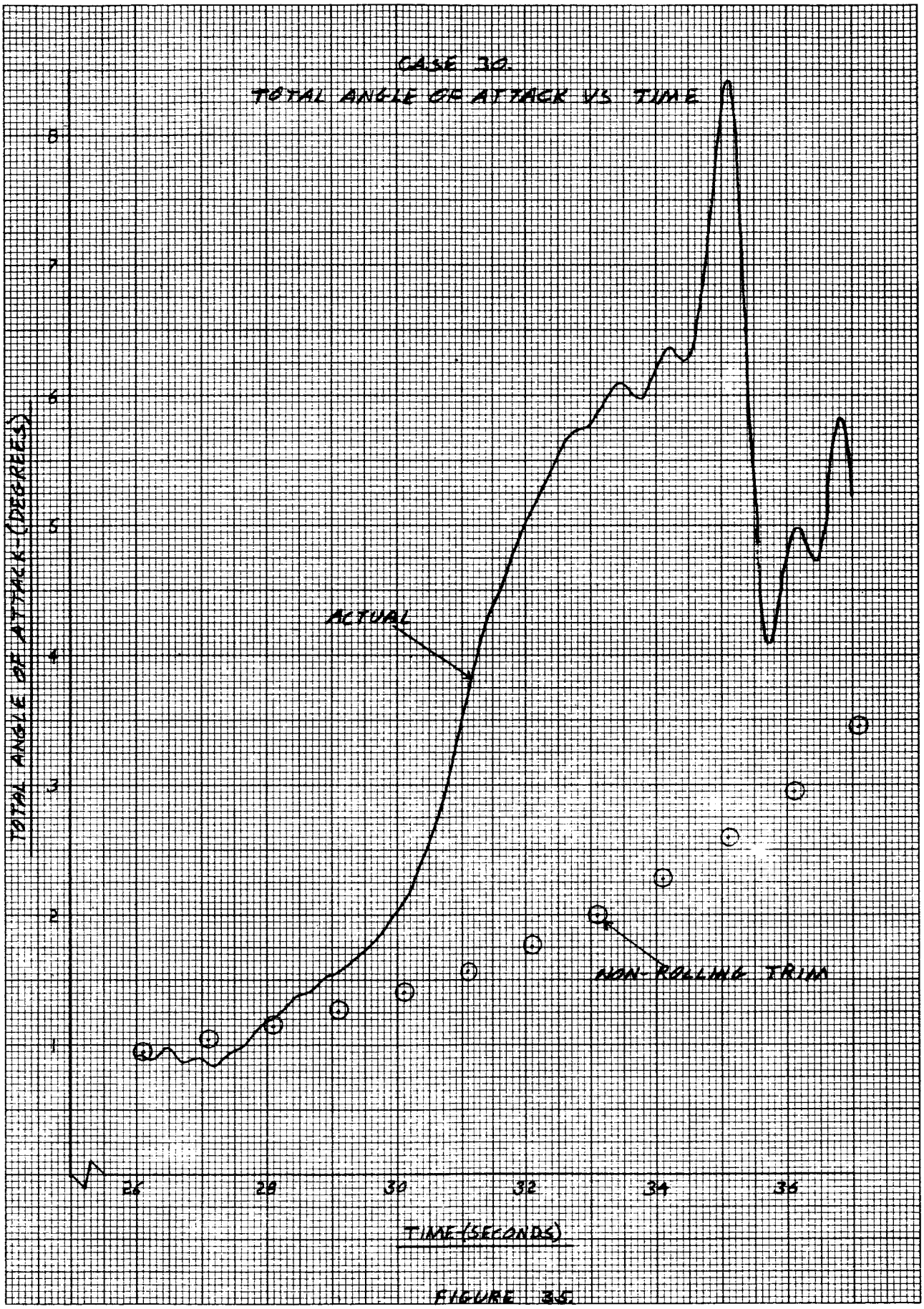
CASE 30.
TOTAL ANGLE OF ATTACK VS TIME
TOTAL ANGLE OF ATTACK-(DEGREES)
8
7
6
5
4
3
2
1
ACTUAL
NON-ROLLING TRIM
26
28
30
32
34
36
TIME-(SECONDS)

FIGURE 35.

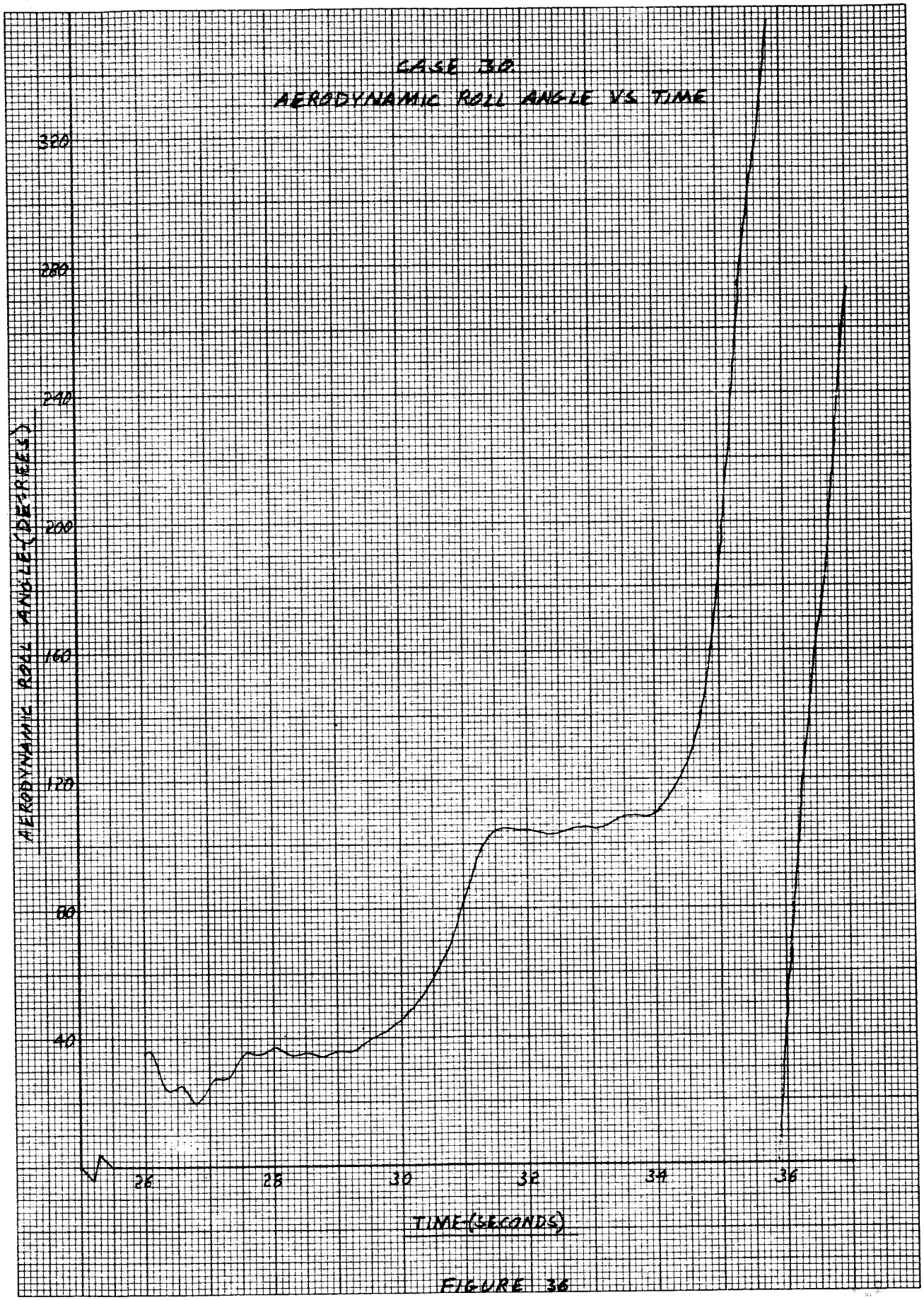
CASE 30
AERODYNAMIC ROLL ANGLE VS TIME
320
280
240
200
160
120
80
40
AERODYNAMIC ROLL ANGLE (DEGREES)
26
28
30
32
34
36
TIME (SECONDS)

FIGURE 36

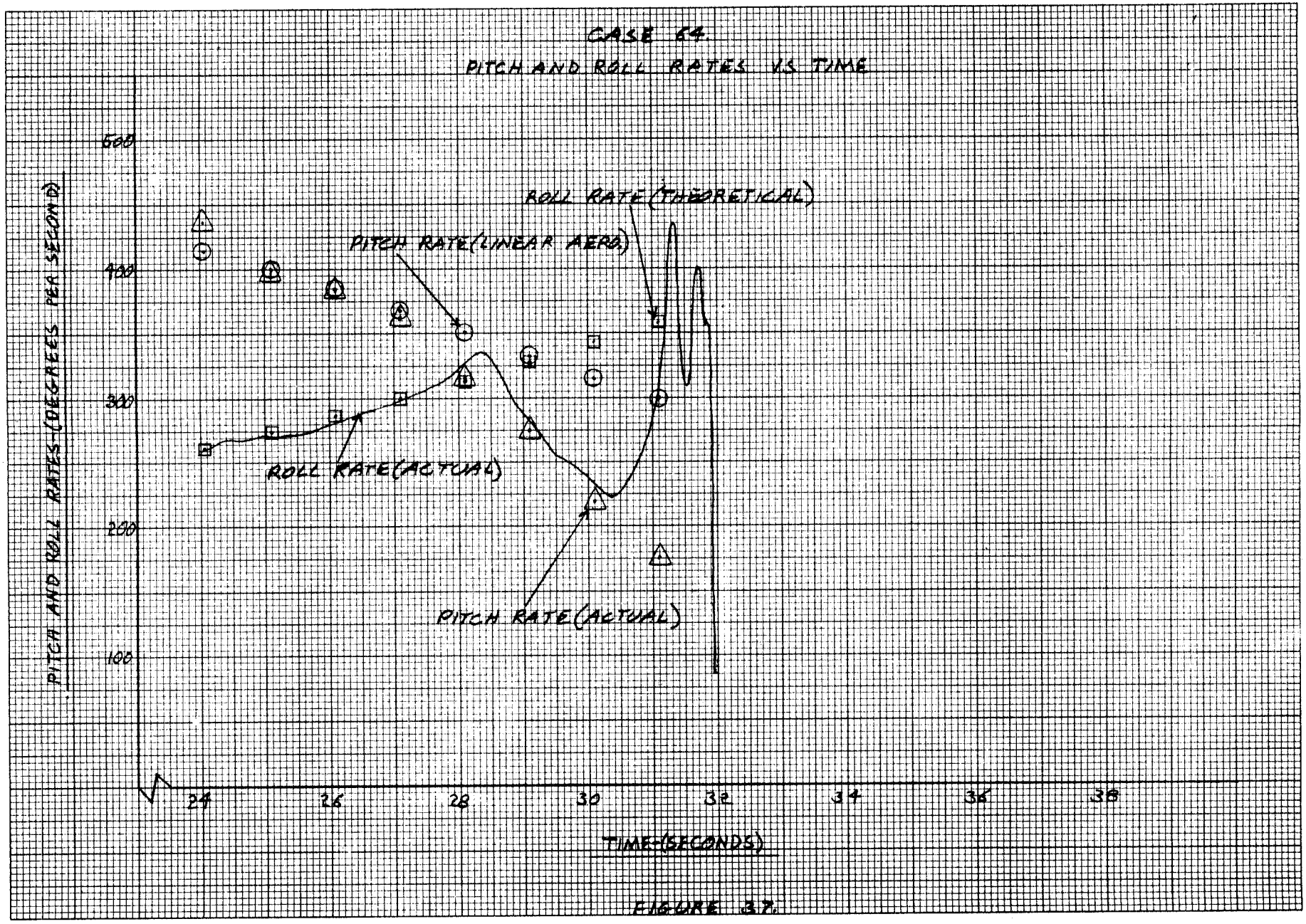
CASE 64
PITCH AND ROLL RATES VS TIME
ROLL RATE (THEORETICAL)
PITCH RATE (LINEAR AERO)
ROLL RATE (ACTUAL)
PITCH RATE (ACTUAL)
PITCH AND ROLL RATES (DEGREES PER SECOND)
500
400
300
200
100
24
26
28
30
32
34
36
38
TIME (SECONDS)

FIGURE 37.

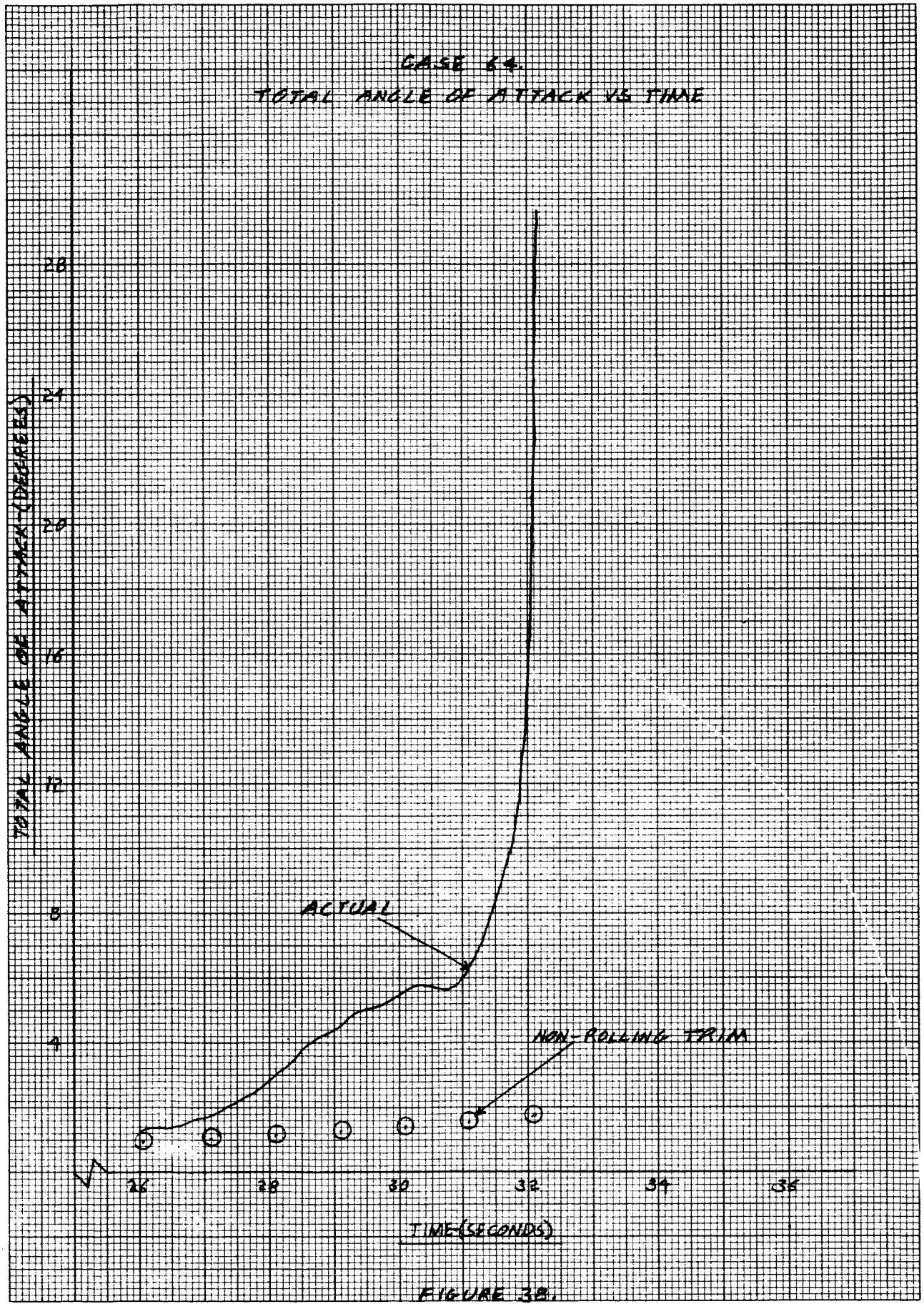
CASE 64.
TOTAL ANGLE OF ATTACK VS TIME
TOTAL ANGLE OF ATTACK-(DEGREES)
28
24
20
16
12
8
4
ACTUAL
NON-ROLLING TRIM
26
28
30
32
34
36
TIME-(SECONDS)

FIGURE 38.

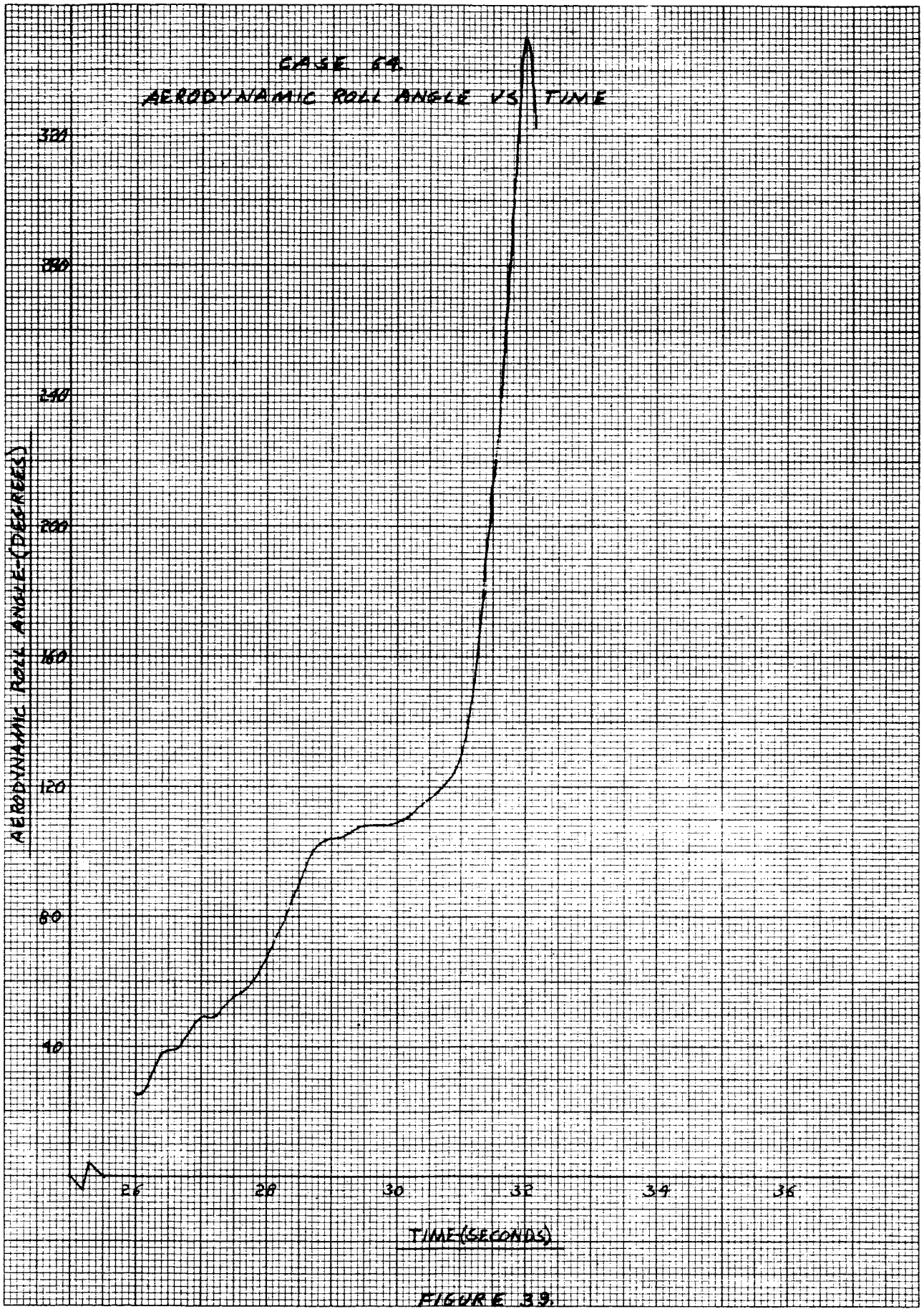
CASE 64.
AERODYNAMIC ROLL ANGLE VS TIME
AERODYNAMIC ROLL ANGLE-(DEGREES)
280
240
200
160
120
80
40
26
28
30
32
34
36
TIME (SECONDS)

FIGURE 39.